INL/EXT-21-62097

# Towards a Robust Sampling Approach: A Computational Review and Design

March 2, 2021

Johan René van Dorp, Tanaya Ulhas Kavathekar, *and* Ekundayo Shittu
*George Washington University*

IES
Integrated Energy Systems

*INL is a U.S. Department of Energy National Laboratory operated by Battelle Energy Alliance, LLC*

INL/EXT-21-62097

# Towards a Robust Sampling Approach: A Computational Review and Design

**Johan René van Dorp, Tanaya Ulhas Kavathekar, and Ekundayo Shittu**
**George Washington University**

**March 2, 2021**

**Idaho National Laboratory**
**Integrated Energy Systems**
**Idaho Falls, Idaho 83415**

**http://www.ies.gov**

**Prepared for the**
**U.S. Department of Energy**
**Office of Nuclear Science**
**Under DOE Idaho Operations Office**
**Contract DE-AC07-05ID14517**

# ABSTRACT

As pointed out in several other works, the estimation of the reliability of the electrical grid can not be conducted without the estimation of the stochastic phenomena of electicity demand and electricity production by variable renewable sources. Therefore, sampling procedures have become integral in the design of engineering structures and analysis. Commonly referred to as Monte Carlo uncertainty analysis or integration, the general objective of these procedures is to establish specifics about the uncertainty of an output characteristic of such an engineering system, given uncertainty about its input characteristics. These sampling procedures are applied in a context in which establishing such specifics cannot be performed through other means. Variance-reduction techniques are designed to lessen the variability among estimators to estimate statistics of those output uncertainties. Importance-sampling techniques, on the other hand, are designed to reduce the number of samples needed to estimate a particular statistic—e.g., a tail probability. The combination of these approaches can reduce the computational burden considerably for a particular estimator and statistic. Importance sampling—geared and designed as it is toward improving a particular estimator—suffers, unfortunately, from the unintended consequence of reducing the performance of other estimators in terms of their variance. The objective of this paper is to offer an alternative sampling procedure where this variance does not grow unacceptably large for a suite of estimators. Moreover, it is anticipated that, with additional knowledge of how an engineering output characteristic responds to its input characteristics, tuning parameters of the input's sampling procedure can be set to improve the output characteristic's estimation. This work proves the effectiveness of the suggested alternative approach. Such positive outcome will lead to a decrease of the computational burden of performing stochastic optimization of integrated energy systems (e.g., components dispatch, and portfolio composition). In particular, capturing the contribution to the overall system cost of rare and unlikely events and patterns of the electricity demand and production will become less computationally expensive. This is due to the fact that the approach demonstrated here will allow the sampling of those rare occurrences more frequently without misrepresenting their probabilistic impacts.

# ACKNOWLEDGEMENTS

The authors would like to acknowledge the funding support of the Department of Energy (DOE) through Idaho National Laboratory (INL) for this project. In particular, we would like to thank Cristian Rabiti, Paul Talbot, and Andrea Alfonsi for being our technical points of contact in the execution of the project. We also wish to express our appreciation to the other members of the bi-weekly team meeting at INL. The opinions expressed in this report are those of the authors and do not reflect the position of the DOE or INL.

# CONTENTS

# FIGURES

# TABLES

# Towards a Robust Sampling Approach: A Computational Review and Design

## 1. INTRODUCTION

The availability of inexpensive electricity, generated by variable renewable, has led to an increasing penetration of those suppliers. While initially this led to a decrease of the overall cost of meeting electricity demand, nowadays it is uncertain if this trend will continue to be the most economical choice. Those doubts are due to the not dispatchable nature of those sources. As a path forward to ensure that more and more variable renewable can be economically integrated into the grid, it has been suggested [1] to deploy a new energetic paradigm usually addressed as Integrated Energy System. In fact, those systems would be able to cope better with the volatility of variable renewable sources. In particular, the DOE-NE funded program Crosscut Technology Development (CTD)–IES has proposed scenarios where nuclear energy is used as a base supplier of energy, while the volatility of the variable renewable is absorbed by an ecosystem of energy user. These IESs would enable a deep decarbonization of the electricity production and of several industrial applications.

Assessing and optimizing such systems is a quite daunting challenge. In particular, in addition to classical challenges tackled by capacity expansion software as ReEDS [2] and production costing software like PRESCIENT [3], trying to capture in full the stochastic nature of the problem requires new approaches. As presented in [4], CTD–IES has developed methodologies to re-create synthetic data that possess the same pattern as the original data and the same statistical property. Those synthetic data representing variable renewable generation, electricity prices, and demand are used to perform stochastic analysis and optimization of IES. In particular stochastic and/or robust optimization requires to access to thousands of prototypical years' worth of data. The methodology developed under CTD-IES allows the creation of such a large amount of data. While this solve the data scarcity problem, it leads to the second challenge, which is the large number of simulation required to perform stochastic/robust optimization. The methodology developed allows for the creation of synthetic data sampling from multivariate correlated distribution. Unfortunately, scenarios (data realization) with very low probability tends to be the most challenging, therefore costly, for the system to cope with, in terms of matching supply and demand. The work illustrated in this report introduces and tests a methodology capable to bias the sampling toward those rare scenarios without most of the penalties introduced when using biased sampling techniques.

As already touched upon, sampling procedures have become integral in the design of engineering structures and analysis. Commonly referred to as Monte Carlo uncertainty analysis orintegration, the general objective of these procedure is to establish the uncertainty distribution of an output characteristic of such an engineering system, given uncertainty distributions of its input characteristics. These sampling procedures are applied in a context when establishing such distributions cannot be performed through other means. The output uncertainty distribution may be referred to as aleatory uncertainty and is akin to the engineering systems response to the uncertain environment in which it operates. This should be contrasted to epistemic uncertainty, which results from lack of knowledge. Generally speaking, epistemic uncertainty can be reduced through the collection of additional data or by increasing the number of samples in a Monte Carlo uncertainty analysis whereas aleatory uncertainty cannot be reduced.

In particular when the establishment of the complete aleatory distribution through Monte Carlo analysis is computationally prohibitive, attention tends to shift towards the estimation of its statistics. Variance-reduction techniques are designed to reduce the variance of estimators to estimate those statistics. Importance sampling techniques on the other hand are designed to further reduce the number of samples needed to estimate statistics, e.g., tail probabilities. While the combination of these approaches can reduce the computational burden considerably, a drawback of importance sampling is that it is geared and designed toward improving a particular estimator with the unintended consequence of reducing the performance of others. The objective of this paper is, in part, to review sampling approaches in a

computational manner while demonstrating their pros and cons. In the process, and in the absence of a mathematical relationship relating an engineered system's output characteristics to its input characteristics, an approach is developed that is geared toward robust performance of an array of estimators of input uncertainties. While this approach will be outperformed by one that is designed for a particular estimator in terms of its variance, the objective is to offer a sampling procedure where the variance does not grow unacceptably large for a suite of estimators. Moreover, with additional knowledge about an engineering system's response to the input uncertainty, tuning parameters of the sampling procedures can be set to improve an output characteristic's estimation of choice.

# 2. LITERATURE REVIEW

Monte Carlo simulation is broadly used in large and complex power-systems reliability evaluation [5] and electricity-demand [6], and risk analysis [7]. However, Monte Carlo requires a huge number of samples to capture rare events with small likelihood. To address this issue, many different algorithms were introduced over the years, such as extreme value theory (EVT) [8][9][10], importance sampling (IS), weighted importance resampling,and general adaptive importance splitting algorithm.

Importance sampling is the process of estimating parameters of distribution using observations from a different distribution. It aims to reduce variance (or other cost function), in which importance ("design") distribution is chosen to obtain estimates of the target distribution. This is demonstrated in the paper "Variance Reduction Techniques for Estimating Value-at-Risk"[11], which analyzes and evaluates quadratic approximation and importance sampling to estimate portfolio-loss probabilities. The numerical results indicate that an appropriate combination of importance sampling and stratified sampling can result in large variance reduction. The largest gains of importance-sampling applications are also seen in the simulation of rare events. The earliest example of importance sampling for rare-event applications dates back to 1951 in the estimation of probabilities of nuclear particles penetrating shields [12]. In importance sampling, the integration estimate is the weighted average of the likelihood ratio of target and importance distribution. These weights do not sum to 1. In the class of problems for which the mean of the output variable is nearly equal to zero, it does not matter whether the sum of the importance weights is not equal to one—for instance, estimating a small probability for which the output variable is 1 if the rare event occurs, otherwise 0. However, it is less successful in other classes of problems. One example is presented by Hopmans and Kleijnen (1979) in the paper, "Importance Sampling in Systems Simulation: A Practical Failure?" In this paper, importance sampling was applied in complicated and dynamic system simulation that resulted in a net-variance increase [13]. As the weights do not add up to 1, the distribution function estimates and complementary probabilities do not add up to 1. In the paper "Weighted Average Importance Sampling and Defensive Mixture Distributions," Hesterberg proposes that including target distribution as one component of the mixture distribution bounds the weights and makes importance sampling more reliable. This method is popularly known as defensive mixture sampling [14].

In the context of energy systems, [15] has proposed a hybrid probabilistic assessment method based on adaptive importance sampling and sequential importance sampling. The proposed method has been tested on the equivalent Australian National Electricity Market. The method shows improvement in terms of accuracy and computational time compared to Monte Carlo simulations.

# 3. UNIVARIATE STRATIFIED SAMPLING

Let the random variable —i.e., is uniformly distribution on the interval from . It is well known that when , where is the cdf of , that:

(1)

Using Equation , one generates a sample from by first generating a sample of size from using a pseudo-random generator and subsequently transforming to a sample of as follows:

(2)

For large values of the sample size the empirical cdf of the sample closely approximates the cumulative distribution function . For a random sample , i.e. and the random variables being mutually independent, and denoting to be an estimator, which is a random variable itself, a sample is seen as a realization of and as a realization of . The sampling distribution of can be obtained computationally from repeated realizations , of that random sample .

A common variance-reduction technique to reduce the variance of is to generate what is called a stratified sample. In that case, the interval is divided into equidistant bins with boundaries and samples are generated independently from , resulting too in a sample from , where now the sample size . Upon transforming the stratified sample to a stratified sample from as per , it assures that each bin , has samples within it. These bins , , partition the support of the random variable in intervals with the same probability mass. The main advantage of stratified sampling in this manner is that low-probability regions within some bin have the same number of samples within it as bins with high-probability regions. The stratified sampling distribution of exhibits a lesser variance than the sampling distribution of using non-stratified samples .

Figure 1A plots the estimated sampling distribution of under regular sampling for using samples , where . It is well known that .

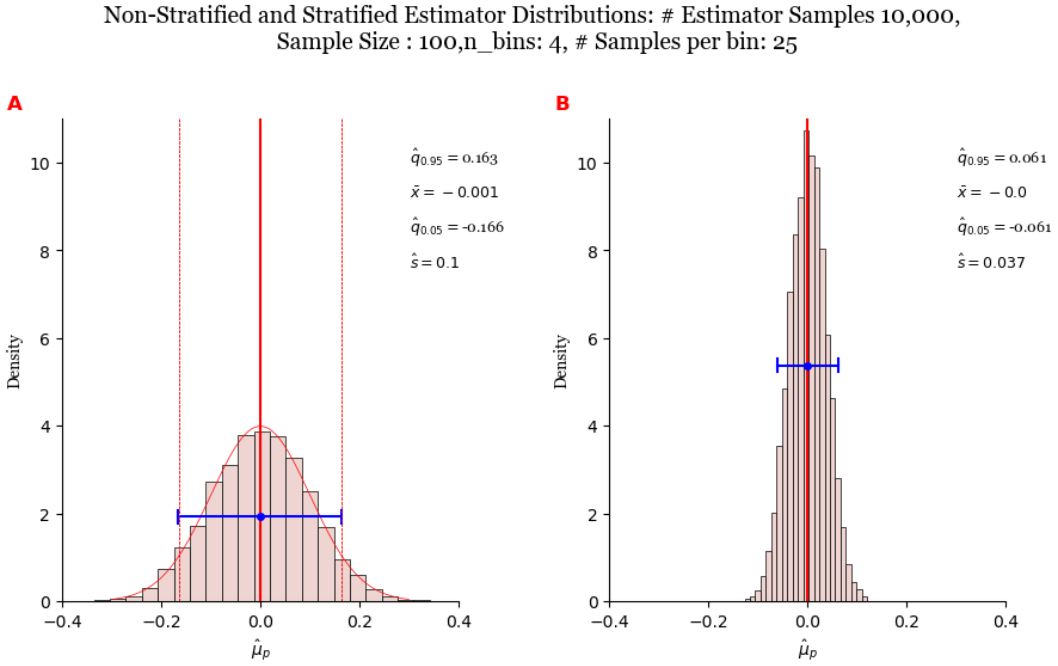


Figure 1. Sampling distributions of , constructed from samples. A: Non-stratified estimator distribution of ; B: Stratified estimator distributions of .

Figure 1A plots that theoretical density function in red. The vertical solid and dashed lines identify the location of the population mean and the location of the th and th percentiles of the density function. On the other hand, the error bar in blue in Figure 1A plots the estimated values for these statistics for under regular sampling, where utilizing samples , where . One observes a close agreement between the estimated and the theoretical values. The estimated values via regular sampling are provided in Figure 1A as well.

Using the same procedure, Figure 1B plots the sampling distribution of under stratified sampling using bins and samples per bin, and stratified samples , where . In Figure 1B the blue error bar indicates the 90% estimated credibility interval for and its sample mean. The values for the estimated th and th percentiles, the estimated mean and standard deviation of , are provided in Figure 1B under that stratified sampling regimen. Comparing the widths of the estimated credibility intervals in Figure 1A and Figure 1B and the standard deviation estimates, one observes about a reduction in uncertainty of the stratified estimator as compared to the non-stratified one. This implies a variance reduction factor of about . Larger reductions will be observed when increasing the number of bins , while keeping the sample size fixed at .

# 4. IMPORTANCE SAMPLING

Conceptually, importance sampling is a process where one samples from an *importance density function*, say , to estimate , where and is the *target density function*. As per the target density one obtains that

(3)

Using a non-stratified or stratified sample from , one traditionally estimates

(4)

The sole purpose of sampling from instead of to estimate , is to ensure a larger number of samples from a low-probability region of the target density when such a low-probability region plays a central role in the estimation of . For example, when , where is the th quantile of and, say, , one evaluates that, in the case of a traditional sampling approach, the expected number of samples to obtain a non-zero estimate of using equals samples. By sampling from an importance density function, say , with a high probability region at that number of samples can be reduced, increasing computational efficiency, but of course, a modification of is required in that case to estimate .

To estimate by sampling from an importance density , one rewrites as follows:

(5)

Denoting to be a random variable with importance-density function and to be a random sample of size , where one obtains the estimator

(6)

Comparing and , one observes that, in , each value is multiplied by a weight , which is referred to as its *importance weight*. One obtains

(7)

In other words, is an unbiased estimator for . That being said, the performance of any unbiased estimator is typically measured by its efficiency, or its variance. One obtains with the independence of , that

(8)

where

(9)

From the right hand side in one observes that in regions where

(10)

the denominator in is close to zero, reducing the value of . On the other hand, in regions where is close to zero, but lacking property , the value of is amplified. [16] states these are the predominant reasons why importance sampling can succeed or fail to estimate . It should be noted that for , is, in fact, a density function, and one obtains from in that case [16]. However, no importance sampling is needed in that instance because would have to be known to evaluate . That being said, the density , which minimizes the variance , is proportional to [17]. From the above, it can be concluded that importance densities are designed to estimate , where is a particular function. In what follows, we will investigate and demonstrate computationally the efficiency of the estimator using different functions , while keeping the importance density fixed.

## 5. DEMONSTRATING IMPORTANCE SAMPLING EFFICACY

From a realization of the random sample one obtains the following estimate from

(11)

To estimate , one sets in . In the case that, is a multimodal distribution, it may be beneficial to follow an importance-sampling approach. To estimate the variance , one sets where equals the importance mean estimate for . Dividing in by instead of reduces that variance estimate to the traditional non-biased moment estimate when —i.e., when the importance distribution equals the target distribution. To estimate the left tail probability , one sets , where

(12)

Defining for a given sample from the importance random variable , the order statistics

(13)

one may obtain an estimate for the empirical cumulative distribution function of using the indicator functions

(14)

as follows

(15)

Observe from that substitution of yields:

(16)

Where, in , is the sample average of the importance weights . Setting in , the sample for is a sample for and, as a result, . Substitution thereof in yields the traditional empirical cdf estimate and . On the other hand, for it follows that , which is a further indication that an importance estimate using Equation , may result in a poor-performing estimate. That being said, it does follow from that

(17)

provided the support of the random variable equals that of the random variable . That being said, a large number of samples may be needed from for , which defeats the purpose of importance sampling. In fact, as mentioned previously, the preferred choice of an importance distribution to estimate depends on the function ) and the value of one attempts to estimate.

The efficacy of importance sampling estimation of is demonstrated computationally in a series of figures and for different functions ) using as the target random variable , hence , and as the importance random variable for different values of . A non-stratified sample from is used, while recognizing that here, too, the stratification approach of Section 3 can be used as a variance-reduction technique. In Figure 2, .

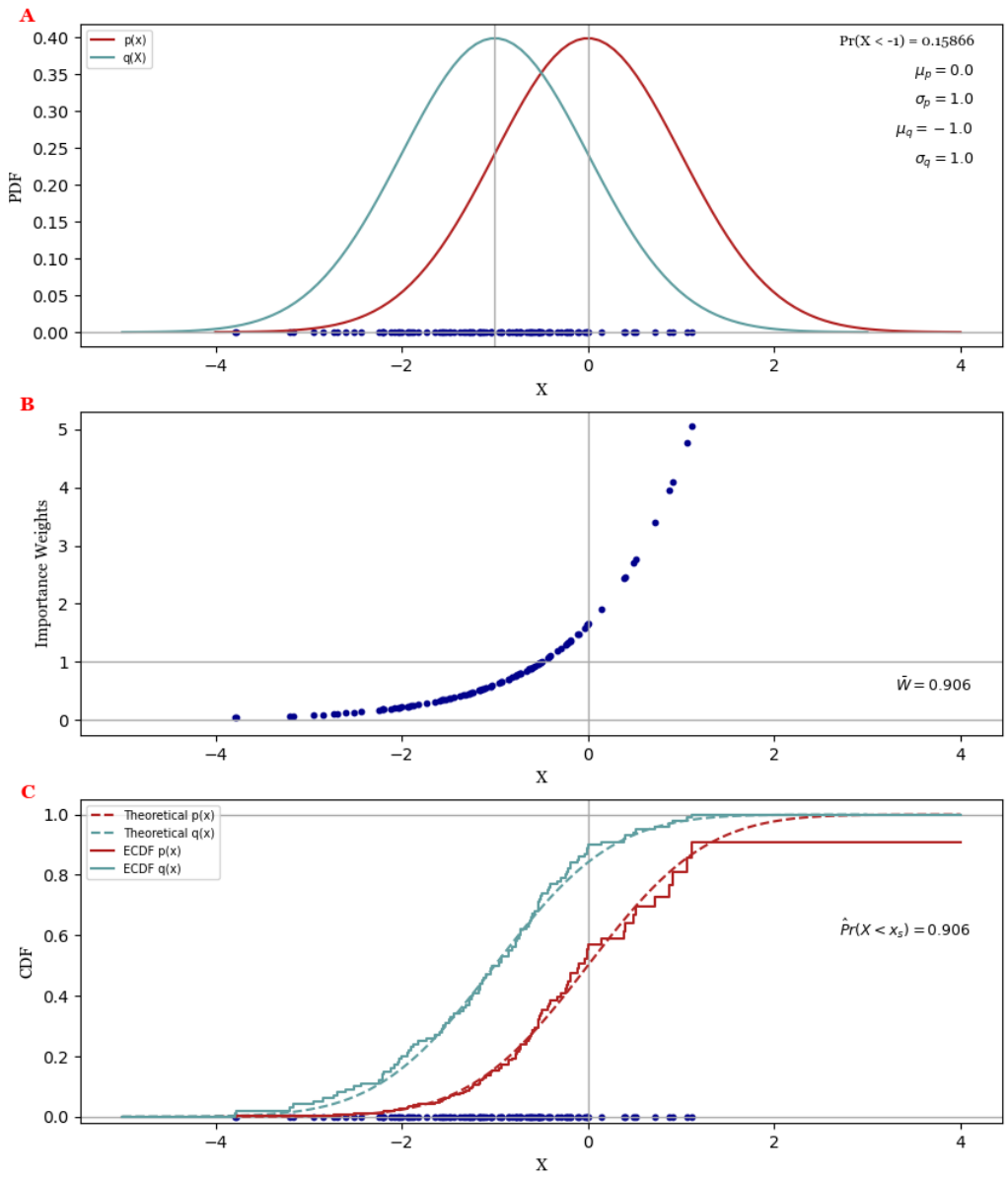


Figure 2. Importance sampling example with target density and importance density . The importance sample , is plotted on the horizontal axis in panels A and C. A: Density functions in red and in blue; B: The importance weights ; C: cdfs plotted with dashed red line with dashed blue lines together with empirical cdf (in blue) and the empirical importance cdf (in red).

The target standard normal pdf is indicated in dark red in Figure 2A; the importance normal pdf with is indicated in blue. The theoretical values of and are provided in Figure 2A as well. The non-stratified importance sample , is plotted in Figure 2A and 2C on the -axis. Figure 2B plots the importance weights and the sample average of these importance weights. The moment-estimators values , , are indicated in the subtitle, together with the importance estimates , , evaluated using . The classical empirical cdf is plotted in blue in Figure 2C, together with the theoretical cdf . The importance empirical cdf , evaluated using , is plotted in Figure 2C as well as together with the theoretical standard normal cdf . Finally, the

estimated value of  is provided in Figure 2C. Note that its value equals the value of  in Figure 2B.

Figure 3 is a version of Figure 2, except that in Figure 3 . In other words, in Figure 3, —i.e., the target density equals the importance density. Observe from Figure 3B that the importance weights . Observe from Figure 3A and Figure 3C that the theoretical pdfs and cdfs align. Observe in addition from Figure 3C that the classic empirical cdf  equals the importance empirical cdf  evaluated using . Finally, the moment estimates and their associated importance estimates in the subtitle in Figure 3 are all equal in value. Summarizing, Figure 3 serves as a verification of the code implemented in  [18] and Python [19] to generate Figure 2.

In Figure 4 sampling distributions are plotted using  non-stratified samples ,  and . Hence, as in Figure 4, the importance density  equals the target density . Figure 4A therefore plots the sampling distribution of  similar to Figure 1A. The vertical dashed lines in Figure 4A are the theoretical th and th percentiles. The error bar end points, in blue, are the empirical th and th percentiles, estimated from the samples. Figure 4B plots the theoretical sampling distribution of  in red. It is well known that . Observe from Figure 4B that the theoretical distribution of  closely matches the empirical histogram for constructed from the  samples , .

Observe a similar closeness with respect to the vertical dashed red lines in Figure 4B and the empirically estimated error-bar in blue, as in Figure 4A. Figure 4 plots the sampling distribution of the estimator , . In the case of Figure 4C, each estimate for  equals to , where  is a realization of ,  because, in Figure 4C, . The sampling distribution of  is well approximated by a normal distribution with mean  and variance , which is the red distribution plotted in Figure 4C. Note that here too the 5th and 95th percentile of that normal distribution in Figure 4C closely matches the empirically estimated 5th and 95th percentile for , —i.e., the end-points of the error-bar in blue. Finally, Figure 4D plots the sampling distribution of  given by , which, of course, equals a degenerate distribution with a single point mass at  because ; therefore, each sample ,  is a sample , , . The purpose of presenting, in detail, both the empirical and theoretical sampling distributions in Figure 4 is that the same code to obtain the empirical sampling distribution in Figure 4 is used to plot the empirical sampling distributions when the importance distribution —i.e., the target distribution.

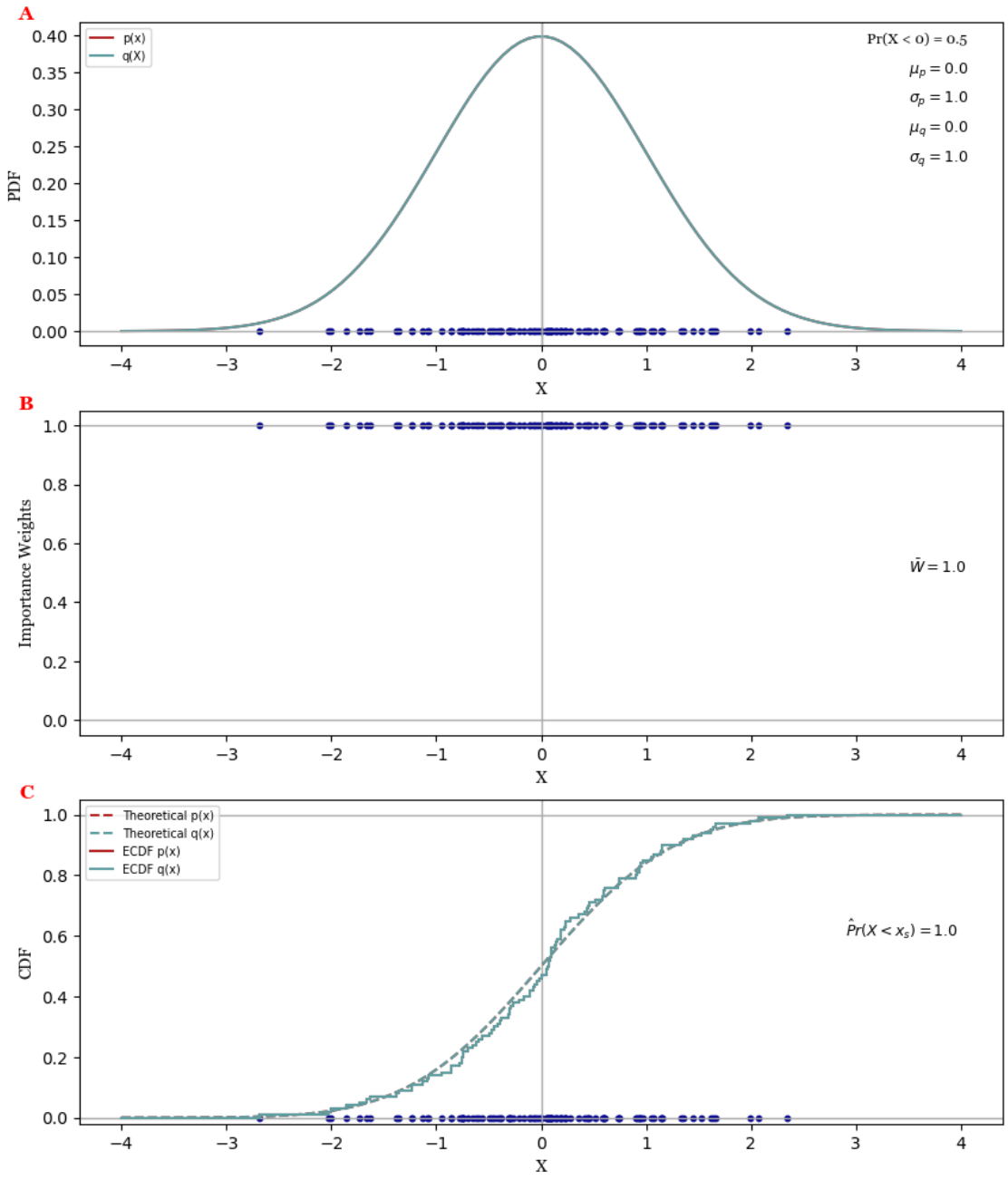


Figure 3. Importance sampling example with target density  and importance density . The importance sample ,  is plotted on the horizontal axis in panels A and C. A: Density functions  in blue; B: The importance weights ; C: cdfs  plotted with blue dashed line together with empirical cdf  (in blue) and the empirical importance cdf  (also in blue).

The differences observed in the empirical sampling distributions in those figures demonstrate the effect of importance sampling on the importance estimates  for the random variable , which are known to

be realizations of unbiased estimators similar to the non-importance estimators plotted in Figure 4. The difference in these importance estimators will primarily be observed by their variances, i.e., by their efficiency.

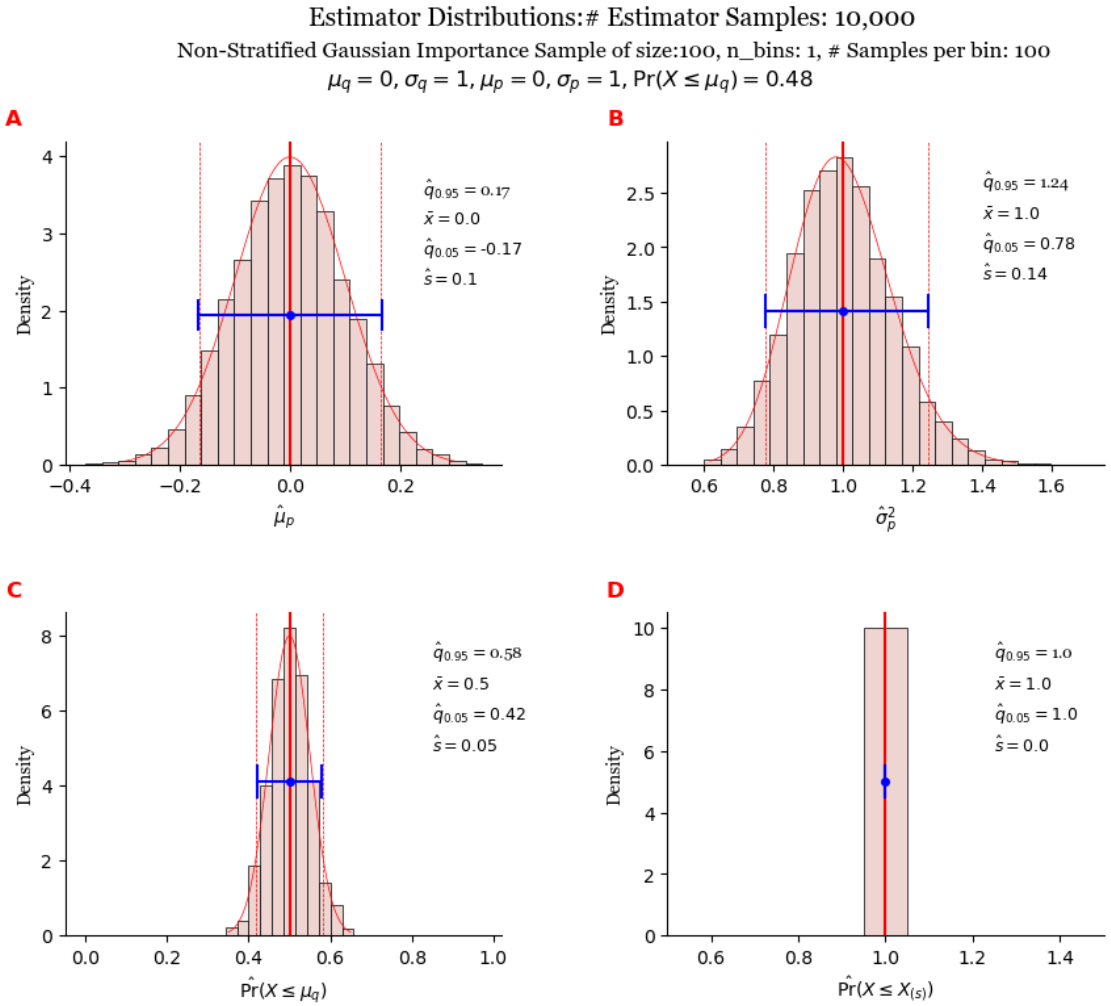


Figure 4. Sampling distributions constructed from  using a non-stratified sample , , where . A: Sampling distribution of ; B: Sampling distribution , ; C: Sampling distribution of , ; D: Sampling distribution of .

Figure 5 is similar to Figure 4, except that in Figure 5, the average of the importance distribution  is set to , and the theoretical pdfs of the sampling distributions are not plotted. Comparing the estimator distributions in Figure 5A and Figure 5B to their counterparts in Figure 4, one observes more asymmetry in their shape in Figure 5. Moreover, one observe a factor increase in the standard deviation from Figure 4A to Figure 5A equal to  (coinciding with a factor increase for the variance of about . In other words, the importance estimator for  in Figure 5A, is less efficient than the traditional moment estimator in Figure 4A. In the case of Figure 5B, one observes a factor standard deviation increase of  (coinciding with a factor increase for the variance of about ). Because Figure 5C plots the estimator distribution of , and Figure 4C plots the estimator distribution of , we compare their coefficients of variation /. For the coefficient of variance of Figure 4C, one obtains the value . For the coefficient of variation of Figure 5C, one obtains an estimated value of , which is similar in value as the coefficient of variation in Figure 4C. Finally, one observes from Figure 5D that the estimator  is not a degenerate distribution, as is the case in Figure 4D, with an average of about , but now a standard deviation of .

Figure 6 is similar to Figure 5, except that in Figure 5 the average of the importance distribution is set to . Moreover, one observe a factor increase in the standard deviation from Figure 4A to Figure 6A equal to (coinciding with a factor increase for the variance of about while the sample mean of the estimator distribution in Figure 4A equals . In the case of Figure 6B, one observes a factor standard deviation increase of .

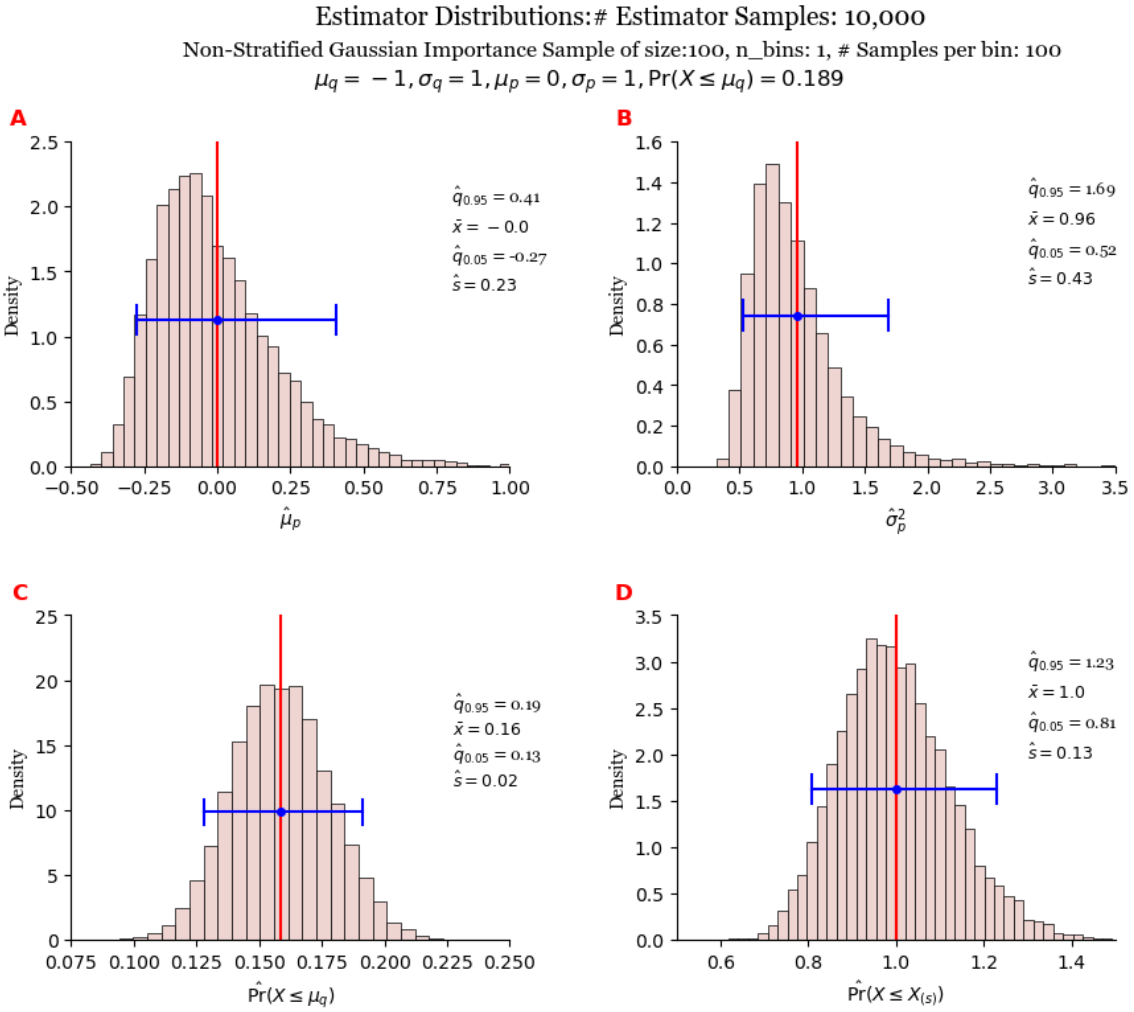


Figure 5. Sampling distributions constructed from using a non-stratified samples , . A: Sampling distribution of ; B: Sampling distribution ; C: Sampling distribution of , ; D: Sampling distribution of .

Moreover, observe from Figure 6B that the mean estimate of as indicated by the blue dot is outside the estimated % credibility interval indicated by the blue error bar. This is indicative of a very long right tail of the estimator distribution also evidence by the large standard deviation . From Figure 6C one estimates a coefficient of variation for the estimator equal to which is still in the same ball park of the coefficient of variations of Figure 4C and Figure 5C equal to and , respectively.

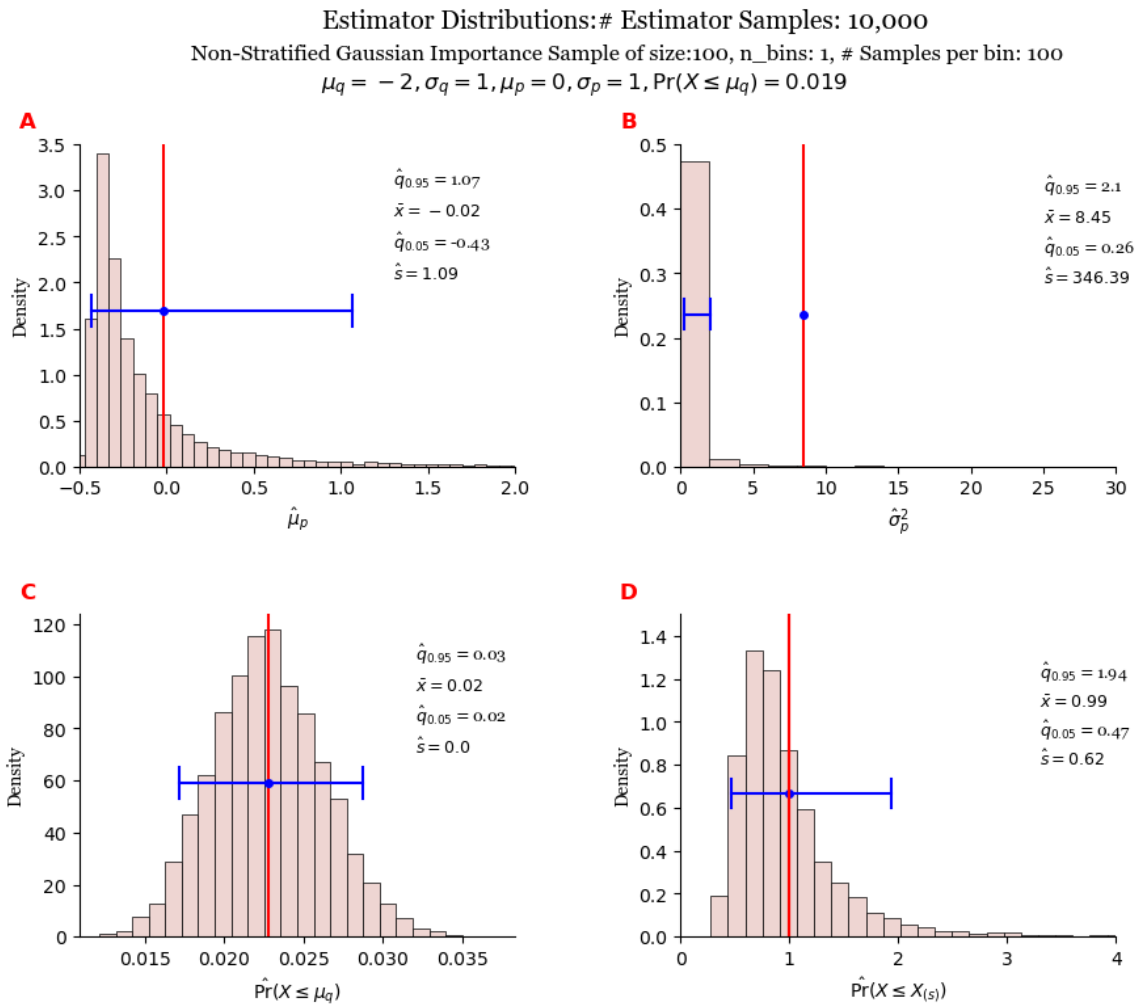


Figure 6. Sampling distributions constructed from using a non-stratified samples , . A: Sampling distribution of ; B: Sampling distribution ; C: Sampling distribution of , ; D: Sampling distribution of .

Observe from Figure 6C that the estimated mean of the estimator distribution equals while the mean of the estimator distribution of in Figure 6D , its standard deviation is a factor larger than the standard deviation in Figure 5D (coinciding with a factor increase for the variance of about . In summary, the only well-performing estimator in Figure 6 is the one for the tail probability . The variance increases for the estimator distributions in Figure 6A, 6D and in particular 6B are such that these importance estimators are particularly inefficient as compared with their counter parts in Figure 4. As one decreases , these effects, demonstrated in the figure panels A, B and D, will only be amplified.

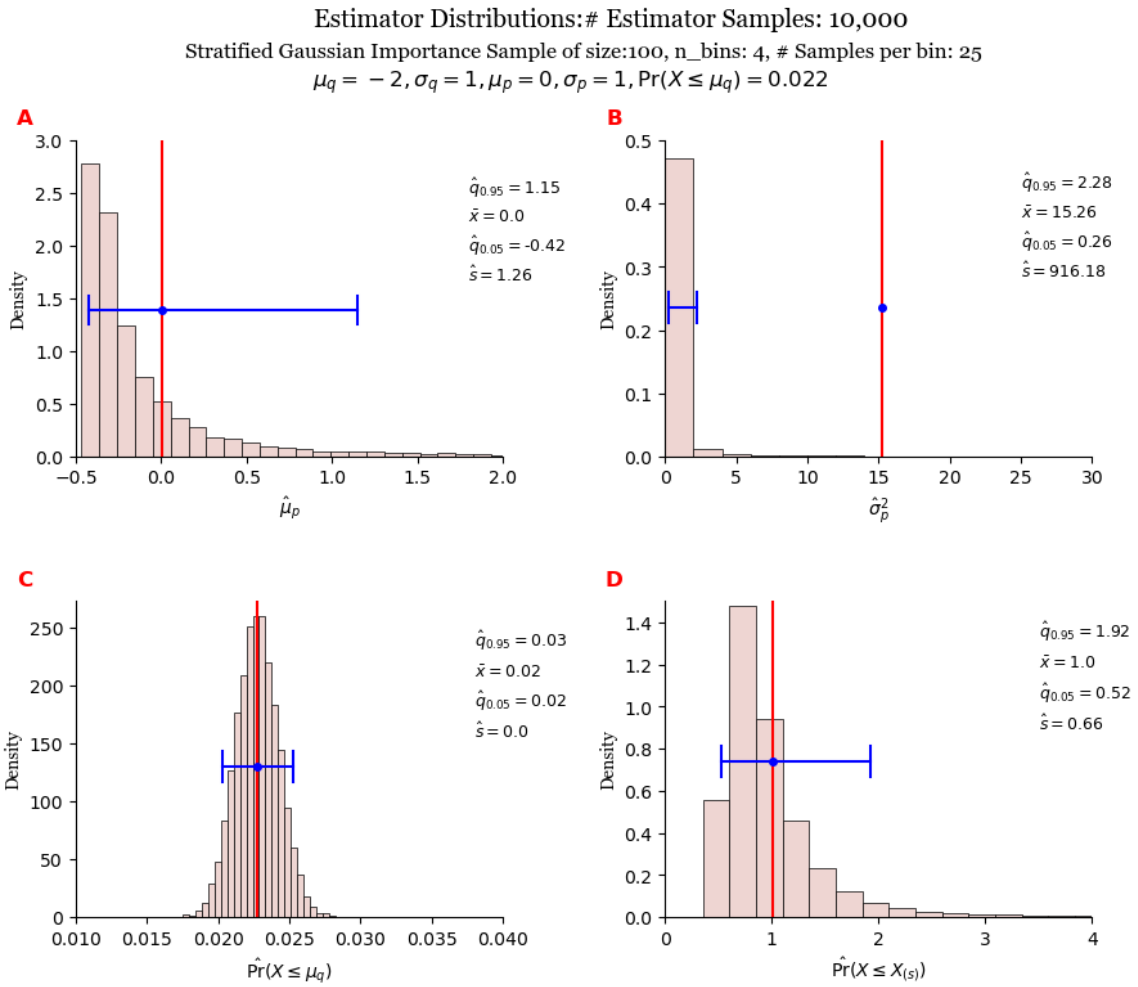


Figure 7. Sampling distributions of importance estimators constructed from stratified samples , , # samples per bin . A: Sampling distribution of ; B: Sampling distribution ; C: Sampling distribution of , ; D: Sampling distribution of .

In summary, it follows from the computational analysis above that, while importance sampling allows one to efficiently estimate small tail probabilities with a small sample size (in Figure 6C only samples were needed to estimate a tail probability of ), the effect on the other estimators in terms of their variance is prohibitive. While one would perhaps expect that stratified sampling could improve the performance of the estimators in Figure 6, a quick comparison of Figure 6 and Figure 7 with estimator distributions constructed from stratified samples using bins and samples per bin demonstrates only an improvement in performance of the estimator in Figure 7C compared to the estimator in Figure 6C. A similar improvement was observed in Figure 1 when using stratified sampling over non-stratified sampling. In others words, a different sampling approach is needed than importance sampling should one have as its objective the estimation of tail probabilities while maintaining a reasonable efficiency of performance in the estimation of the other estimators in Figure 4, Figure 5, Figure 6, and Figure 7.

# 6. UNIVARIATE UMBRELLA/MIXTURE SAMPLING

As in the previous sections, it is assumed that Hence, the target distribution where , is the classical standard normal density. Because, in principle, the objective of our importance-sampling approach is to allow for the estimation of extreme tail probabilities, an importance density is needed for heavier tails than the classical standard normal density function . A popular choice for such a heavier-tailed distribution is a student-distribution with degrees of freedom and variance /. In other words, for the value the variance of that student- is three times that of a standard normal distribution. Denoting the ratio of tail probalities and by , where and i.e.,

. (18)

Figure 8 plots as a function of . One observe from Figure 8 that for and , it is more likely to obtain a sample in in the left tail than it is in the left tail . Moreover for , it is equally likely, naturally, because both the student- and the standard normal distribution are symmetric around their mean . One obtains for :

(19)

In other words, for a sample size of , one expects samples in the left tail of and sample in the left tail of . For larger values of , the number of samples expected in the left-tail would be less.

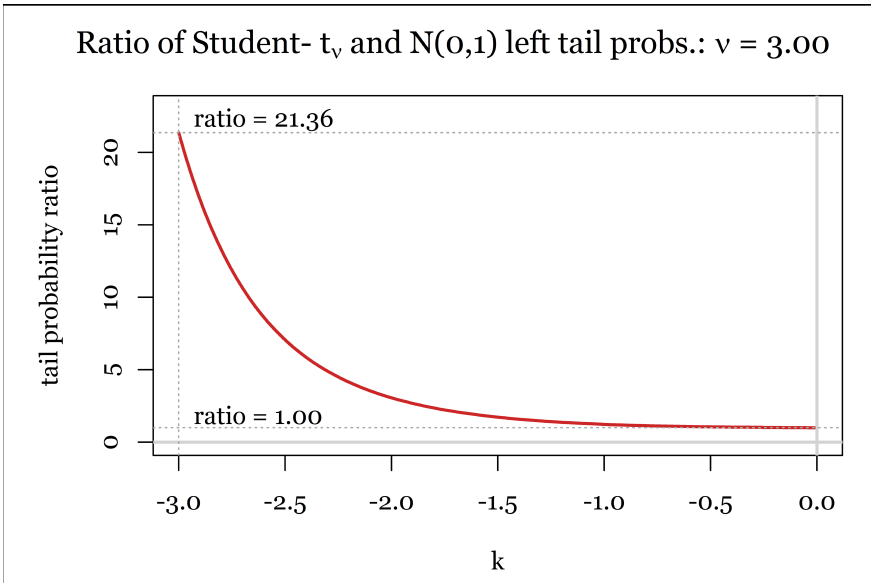


Figure 8. Ratio as a function of , where and .

To allow for importance sampling with a higher ratio of , for example, a univariate density is constructed using a mixture technique. That is, the importance distribution will be of the from

(20)

The mixture weights , in can be considered tuning parameters of the importance distribution . The second member is set equal to the target distribution . One obtains, in that case, for a sample from , the importance weight

(21)

In other words, importance weights cannot become arbitrarily large. The extreme case—where one of the importance weights , and the others weights do not—has the implicit effect of reducing the importance sample size to a single data point, which in turn results, in practice, in a biased estimate given such a sample. Thus, intuitively, a large imbalance in the importance weights reduces the effective sample size of the importance sample [20], resulting in an increased variance of the importance estimator

. Hence, by selecting one of the members in  to be the target distribution, the importance weights have an upper bound , where  is the mixture weight of  in . The latter prevents excessive imbalances in the importance weights, and for that reason, the inclusion of the target distribution in  is termed *defensive* mixture sampling [16].

## 6.1 Gamma Distributions with a Fixed Tail Probability

Based on the objective to estimate , and to separately be able to model heaviness of the right tail of the importance distribution , it is proposed to use a gamma distribution with a mode at  for the third member  in . For the first member,  in , it is proposed to use the reflection of that gamma distribution, which results in a symmetric importance distribution  with symmetry axis  because the target distribution shares that same symmetry axis. The latter implies the same performance of estimating the left and right tail probabilities of the target density . One obtains for the gamma density with pdf

(22)

a mode at ()/ for  and a variance equal to /. Setting the mode equal to  and the variance equal to  yields the following set of equations:

(23)

Using , Figure 9A plots  as a function of  for the values  and , respectively. When the standard deviation  the density  converges to a degenerate distribution with a probability mass of at the mode  and . When the standard deviation , it follows that  because  is held fixed. One observes from Figure 9A that the tail probability  strictly increases as a function of  while keeping  fixed. In other words, one may specify ),  and solve for a unique value of  that matches that tail probability constraint using a standard root-finding algorithm such as *Uniroot* in . The unique values for , given  andand , are provided in Figure 9A. The associated gamma densities are plotted in Figure 9B. The parameter values for the gamma pdf in red in Figure 9B are , , in green are , , and in blue are , . Note that the  parameters are of the same value, whereas the values of the  parameters change.

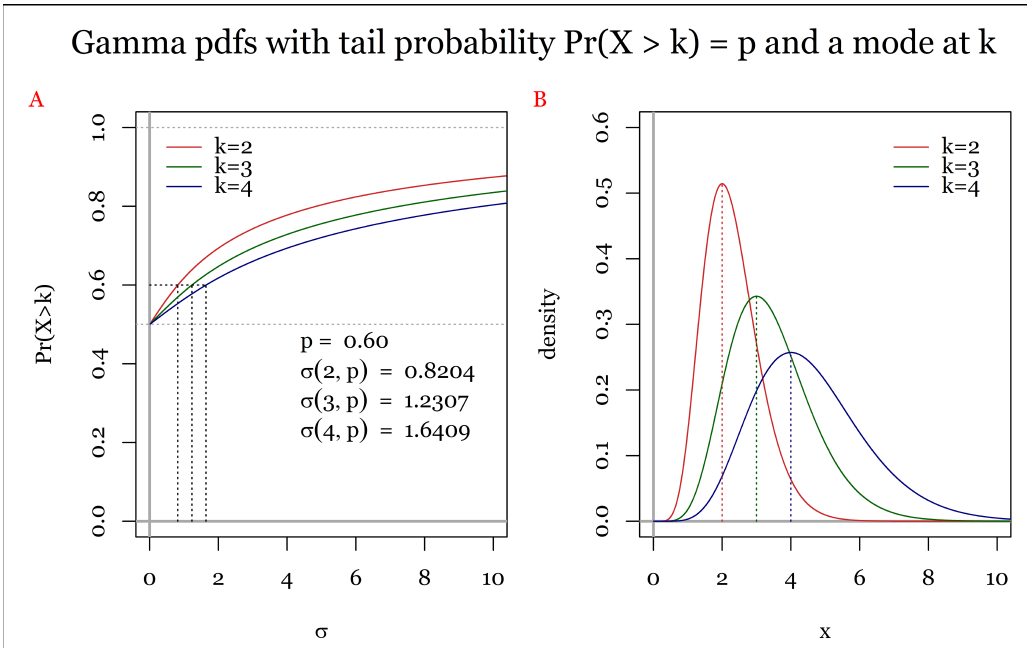


Figure 9. A: Gamma tail probabilities as a function of standard deviation  and a mode at ; B: Gamma pdfs with a mode at  and .

## 6.2 Constructing the Umbrella/Mixture pdf

Let where are the member pdfs of the mixture pdf . Defining for the following probabilities

(24)

and introducing the matrix , one obtains with the vector of mixture weights that

(25)

where . Under a symmetry requirement of , one selects to be the reflection of the . Next, setting in , one obtains , where its first element is an upper bound for the right tail probability (and left tail probability ). Analogously, setting in one obtains , where its first element is a lower bound for the right tail probability . Selecting a value for the left tail probability , under the condition that

(26)

one obtains with the symmetry of that . Next, the mixture weights follow from .

Setting to the gamma pdf in Section 6.1, and to the reflection of , one obtains with the symmetry of with standard normal cdf , and that

(27)

Under condition , one obtains from and for the mixture weights, after some algebraic manipulations,

(28)

Setting and and , one obtains the following mixture weights from :

(29)

The associated mixture pdfs are plotted in Figure 10 in orange and derive their designation *umbrella* pdfs from their shape. The plotted curves in red equal , the plotted curves in green equal , where represents the gamma densities plotted in Figure 9B. Finally, the plotted curves in blue equal , where is the reflections of the gamma densities plotted in Figure 9B. Because in solving for , , it follows from that as . It is worthwhile to note, as a comparison with the ratio ) in Figure 8, that such a ratio of tail probabilities for the umbrella pdf in Figure 10B equals . Hence, it is about 111.12 more likely to obtain a sample in the tail of when sampling from . The value in Figure 8 was evaluated using a student-distribution with degrees of freedom. Finally, for all three importance pdfs plotted in Figure 10A, 10B and 10C, 30% of their probability mass is distributed over both tails, whereas 70% of their probability mass is located in for all three values . In other words, when sampling from the importance densities in Figure 10, in orange, about 30% of the samples will be sampled from their tails. That percentage can be altered by selecting different values for either or . Hence, both parameters can be considered tuning parameters for the umbrella pdf . Alternatively, instead of changing and solving for the vector of mixture weights from , one may specify a weight vector , where .

## 6.3 Sampling from the Umbrella pdfs

To facilitate demonstrating sampling from the umbrella pdf , the mixture weights is selected in , where . Hence, the mixture weight for the target density becomes a parameter of the umbrella pdf developed in the previous sections. The remaining weight is equally split over the tails of the gamma tails of the umbrella pdf to ensure its symmetry. The other parameters of the umbrella pdf are and , which determine the heaviness/fatness of these gamma tails, where and with a mode at (see Figure 8). To generate a realization of a random sample from the umbrella pdf , one first repeatedly generates a sample value from a discrete distribution over , where its probability-mass function is defined by the vector of mixture weights , and next generates a sample from the continuous mixture member . These samples from the members in the umbrella pdf can be sampled in both a stratified and non-stratified manner. Herein, a non-stratified–sampling approach is used to allow for comparison with the results in Section 5.

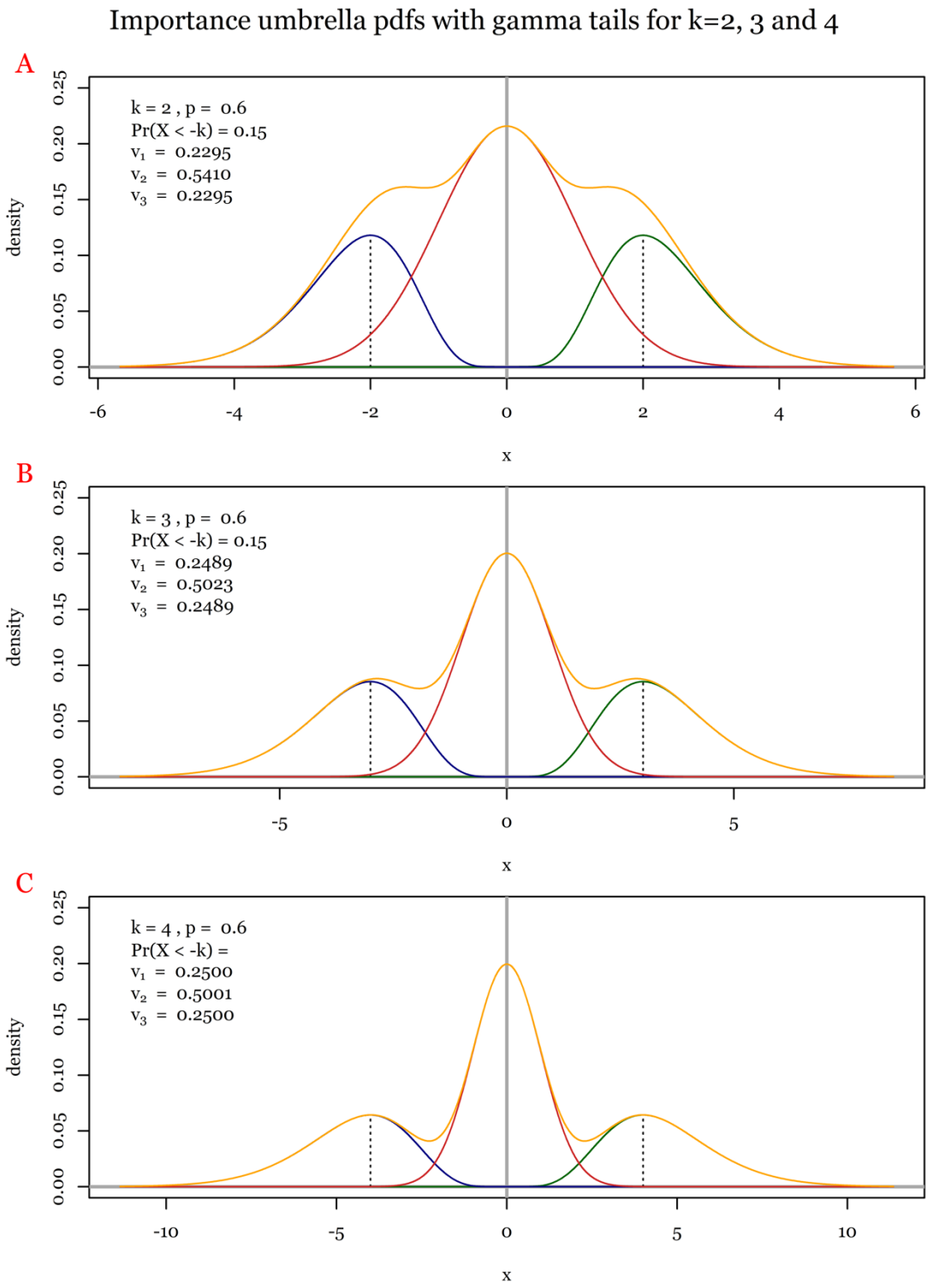


Figure 10. Importance umbrella pdfs in orange, constructed using the mixture weights in and the gamma distributions in Figure 9B.

The next three figures demonstrate importance of sampling by sampling from the umbrella pdfs in Figure 10, with the caveat of the previously described change in mixture weights. Figure 11A plots a

standard sample on the x-axis from a standard normal pdf . Its subtitle lists the population values for the mean , the standard deviation and the sum of the tail probabilities and . Since the sum of those tail probabilities is approximately equal to . Recall the well-known rule of thumb that of the probability mass of a normal distribution is within two standard deviations from the mean. In addition, the subtitle in Figure 11A contains the traditional method of moments estimates for , and the estimate for the sum of these tail probabilities. Observe from Figure 11A that two samples are located in both tails and therefore the estimate follows for that probability in both tails.

Figure 11B plots the umbrella pdf in an orange color and the same gamma distributed mixture members (in blue and green) as plotted in Figure 10A together with the defensive mixture member in red. Samples of size from these gamma mixture members are plotted on the x-axis in the same color together with a sample of size from in red. Hence, these sample size are consistent with the mixture weights and a total sample size of . The importance estimates for the mean, the standard deviation and the sum of the tail probabilities are provided in the subtitle of 11B. Note that their values are comparable to their counterparts in 11A. Finally Figure 11C plots the importance weights for the umbrella sample of size with the importance weights of the sub-samples of the mixture members plotted in Figure 11C in the same color as the mixture member pdfs plotted in Figure 11B. Observe from Figure 11C that the importance weights are bounded from above by as explained using and .

Figure 12 and Figure 13 are similar to Figure 11, except that and , respectively. Observe from Figure 12A and Figure 13A that no samples are observed in the tails or results in the tails probability estimate in the subtitle of these figure panels. Observe from Figure 12B and Figure 13B that the umbrella samples of size do contain samples in these tails of the target density .

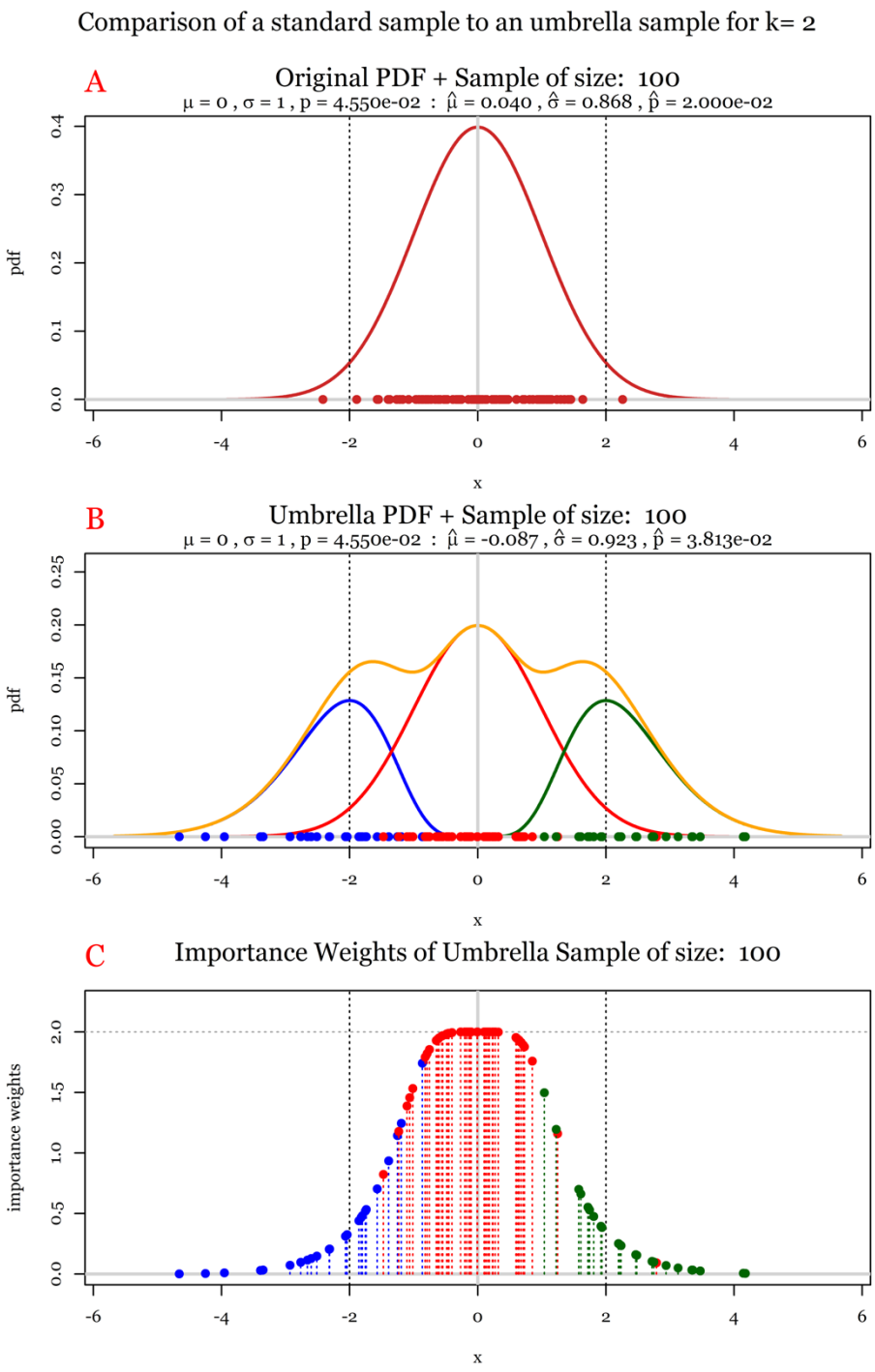


Figure 11. A: Standard normal pdf with regular sample of size plotted on the x-axis; B: Umbrella pdf for in orange color with gamma distributed tails (in blue and green), defensive mixture member (in red) and mixture weights . Samples from the mixture members are plotted in the same color on the x-axis; C: Importance weights of the umbrella sample plotted in the same color as the mixture members of the umbrella pdf plotted in Figure panel B.

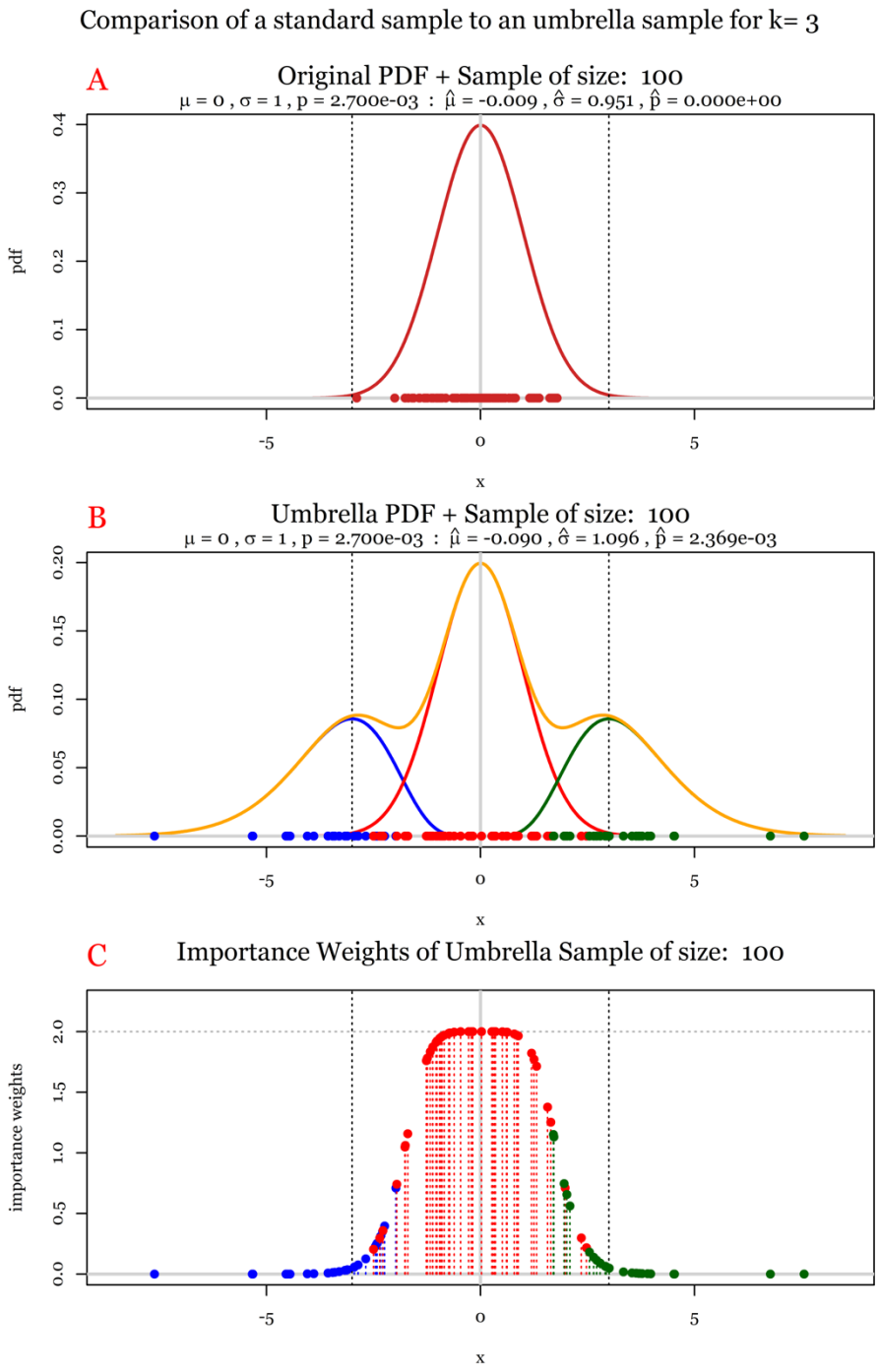


Figure 12. A: Standard normal pdf with regular sample of size plotted on the x-axis; B: Umbrella pdf for in orange color with gamma distributed tails (in blue and green), defensive mixture member (in red) and mixture weights . Samples from the mixture members are plotted in the same color on the x-axis; C: Importance weights of the umbrella sample plotted in the same color as the mixture members of the umbrella pdf plotted in figure panel B.

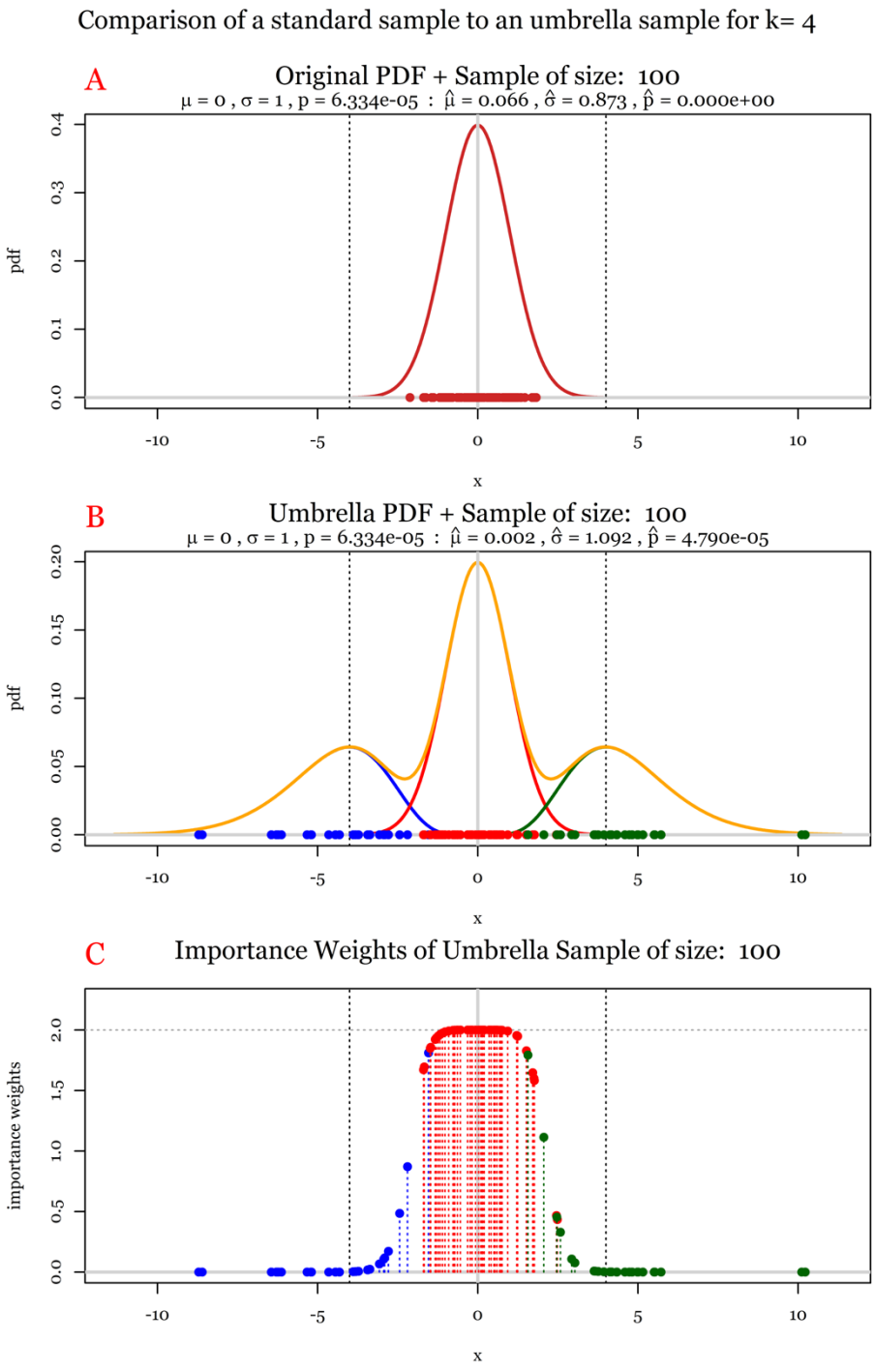


Figure 13. A: Standard normal pdf with regular sample of size plotted on the x-axis; B: Umbrella pdf for in orange color with gamma distributed tails (in blue and green), defensive mixture member (in red) and mixture weights . Samples from the mixture members are plotted in the same color on the x-axis; C: Importance weights of the umbrella sample plotted in the same color as the mixture members of the umbrella pdf plotted in Figure panel B.

In Figure 12B, this results in a tails probability importance estimate  whereas its population value equals . In Figure 13B, the sum of the tail probabilities equals  with an importance estimate  indicated in its subtitle. It is important to note that these importance estimates are obtained using only  samples from the umbrella pdf  . As in Figure 11C, the importance weights in Figure 12C and Figure 13C are bounded from above by the value . Finally, observe that the importance estimates for the population mean and the population standard deviation in the subtitles of Figure 12B and Figure 13B are close to their population counterparts. That being said, while the importance estimate in Figures 11–13 are reasonable, the performance of the importance estimators (of which the estimates in Figures 11–13 are realizations) ought to be evaluated by their distributions or the variances of these sampling distributions.

## 6.4 Univariate Umbrella Estimator Behavior

The umbrella pdf developed in Section 6.2 is used as the importance density in the estimation of . Samples size of  is generated to be consistent with the estimator distribution analysis presented in Section 5. The estimators obtained following this procedure are referred to as umbrella estimators. The sampling distributions of the umbrella estimators for (i) the sum of the tails probabilities, (ii) the population mean, and (iii) the population variance is studied computationally using the umbrella pdfs in Figures 11–13 with a minor modification of the mixture weights in these umbrella pdfs. Their performance is compared to the sampling distributions of classic estimators for these population statistics under regular sampling. The parameters of the umbrella pdf developed in Section 6.2 can be summarized using the parameter vector , where  is the mixture weight in the umbrella pdf  for the target density . The parameters  and  determine the  and  parameters of the gamma mixture members in  as per the procedure described in Section 6.2. In the computational analysis that follows, parameters  and  are held fixed at  and  whereas the value of the parameter  is selected from .

Defining

(30)

Figure 14A studies the sampling distribution of the classic estimator for  using a random sample of size  from . That classic estimator's sampling distribution is a scaled binomial distribution that is well approximated by a normal distribution with parameters  and variance  because, for ,

(31)

The pdf plotted in red in Figure 14A and 14B is that normal distribution. The dashed vertical lines in in Figure 14A and 14B identify the theoretical values of its  and  percentiles. The solid red vertical lines in Figure 14A and 14B are plotted at the population mean . The error bar in blue in Figure 14A identifies the empirical estimates of these quantiles and the sample mean of the sampling distribution for the estimator of  using  estimates  under regular sampling. One observes from Figure 14A that the estimated values of the percentiles and the mean align with their population counterparts. Figure 14B studies the sampling distribution of the umbrella estimator utilizing a random sample of  from , where .

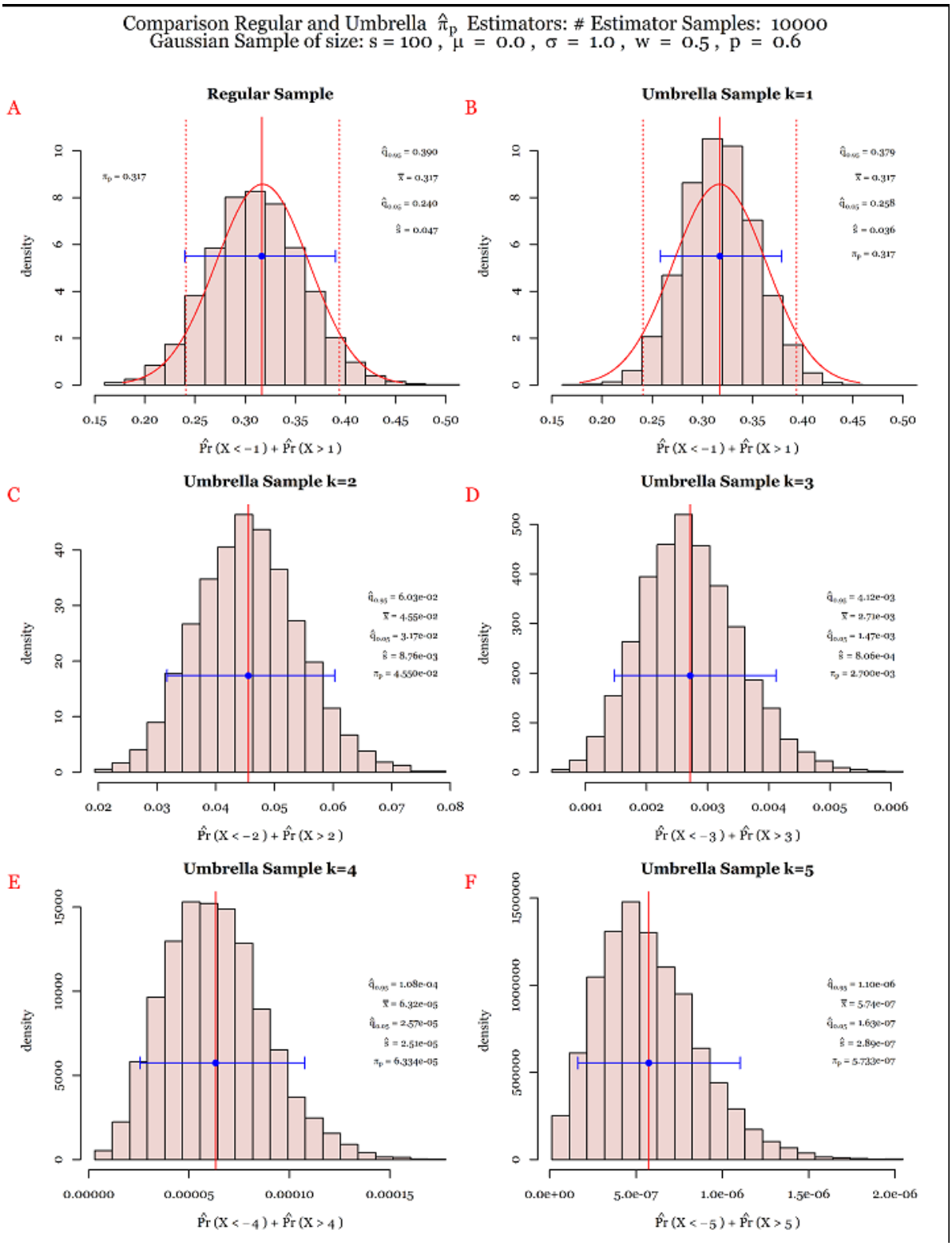


Figure 14. Sampling distributions of estimators , , constructed from samples using regular (A) and umbrella (B–F) non-stratified samples , . A: ; B–F: , for .

Comparing the sampling distributions in Figure 14A and Figure 14B, one observes from the blue error bar in Figure 14B a credibility interval, with a lesser width and a lesser sample standard deviation for the umbrella estimator. Summarizing, the umbrella estimator in Figure 14B outperforms the estimator in Figure 14A under regular sampling from the target density .

Figure 14C–F plot the sampling distributions of the umbrella estimators for . Because in these cases, they cannot be compared to a normal distribution with mean and variance , as was the case in Figure 14B. Their performance can, however, be compared to the coefficient of variation in Figure 14A and in Figure 14B. One obtains, for the coefficient of variation in Figure panels 14C–F, the values , respectively. Because the value of decreases as increases, a reduction in performance of these umbrella estimators, while keeping the sample size fixed, is to be expected. That being said, it is worthwhile to note that in Figure 14F, the sample mean of the empirical sampling distribution, whereas . These values are close, which is indicative that the umbrella estimator in Figure 14F is unbiased, as per . The estimates for to construct Figure 14F were obtained using only a sample size of for each estimate. Under regular sampling, a sample size of million samples would be needed to obtain a single non-zero estimate for . The latter is indicative of the reduction of the computational effort to estimate small tail probabilities via umbrella sampling.

Because umbrella sampling is an importance-sampling method, a reasonable performance of tail-probability estimation is to be expected. That being said, in Section 5 it was demonstrated that using the importance densities therein resulted in what can be considered an unacceptable performance of importance estimators for the mean and the variance of the target density . Specifically, while theoretically these importance estimators are unbiased, as per , their variances increased substantially as increased while keeping the sample size fixed. Figure 15 studies the behavior of the umbrella estimator for the mean for and while keeping the parameters and fixed for the umbrella pdfs. Figure 15A is the same as Figure 4A and plots the empirical sampling distribution of the random sample mean under regular sampling. In addition, Figure 15A plots the theoretical sampling distribution in red, which shows a normal distribution with a mean of and a standard deviation . Observe that the empirically estimated quantiles and sample mean of the estimator in Figure 15A, as presented by the blue error bar, align with their theoretical values (plotted using the vertical dashed and solid red lines).

That same sampling distribution in red is also plotted in Figure 15B–D for comparison purposes. Figure 15B–D plot the sampling distributions of the mean umbrella estimators and thereby compares them to the theoretical sampling distribution of the mean estimator under regular sampling, plotted in red. Because the estimator in Figure 15A is known to be an unbiased minimum-variance estimator for the population mean, one observes, perhaps surprisingly, a similar performance in Figure 15B for as in Figure 15A. A larger standard deviation is observed in the sampling distribution for and in Figure 15C and 15D, respectively. That being said, the sample standard deviation in Figure 15B displays a marked improvement over the standard deviation in Figure 6B. The importance densities used in Figure 15B and Figure 6B were both chosen to estimate tail probabilities that are similar in orders of magnitude. Moreover, one observes that the sample standard deviations and in Figure 15C and D, respectively, are also less than the one in Figure 6B, despite the umbrella pdfs used in Figure 15C and 15D being designed for the estimation of tail probabilities of a lesser order of magnitude.

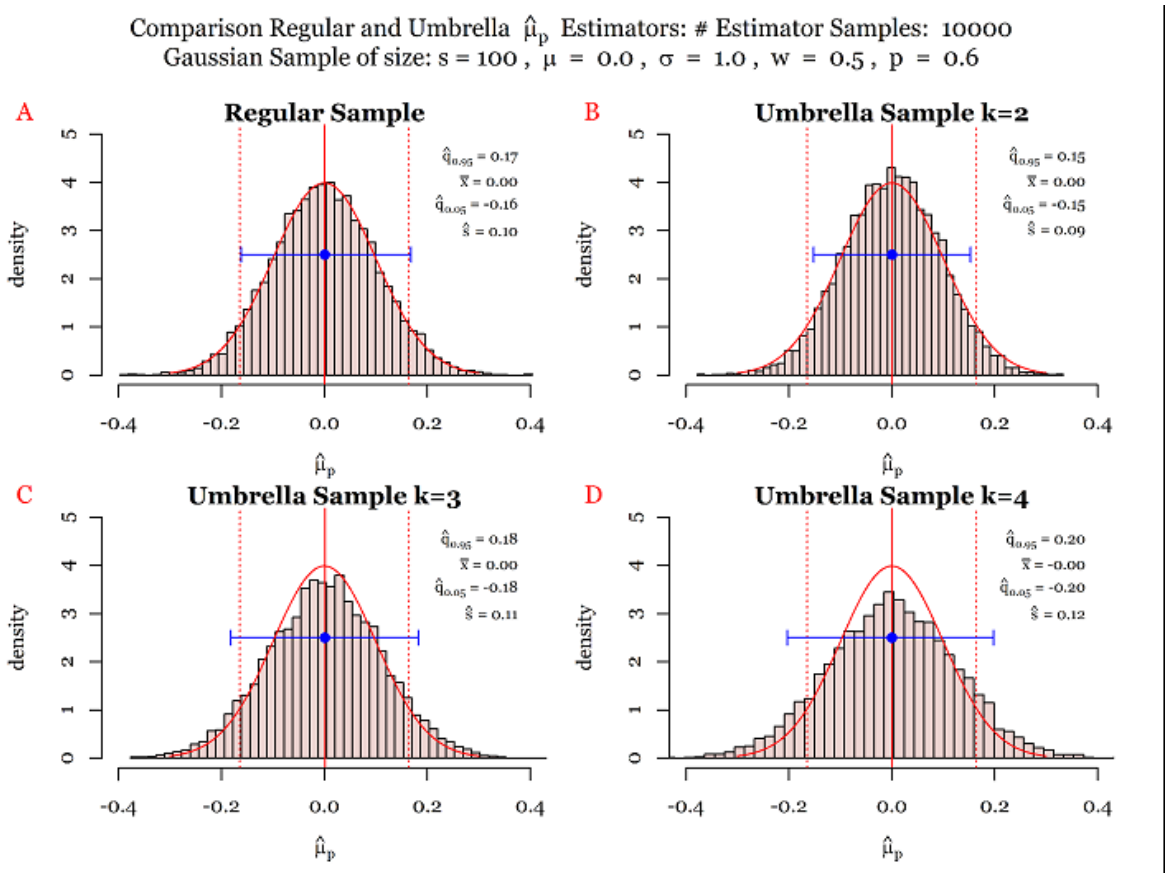


Figure 15. Sampling distributions of mean estimators constructed from  samples using regular (A) and umbrella (B–D) non-stratified samples , . A: ; B–D:  ,  for .

Figure 16A plots the empirical sampling distribution of the variance estimator under regular sampling and is the same as Figure 4B. In addition, Figure 16A plots the theoretical sampling distribution of  in red, where . Observe that the empirically estimated quantiles and sample mean of the estimator  in Figure 16A, as presented by the blue error bar, align with their theoretical values (plotted using the vertical dashed and solid red lines). That same sampling distribution in red is also plotted in Figure 16B–D for comparison purposes. From Figure 16B () and Figure 16C (), one observes that the umbrella estimators outperform the estimator in Figure 16A in terms of their variance. A similar performance in terms of their variance is observed between the umbrella estimators in 16D () and 16A. Also observe that the sample mean estimates in Figure 16B–16D align with the population value .

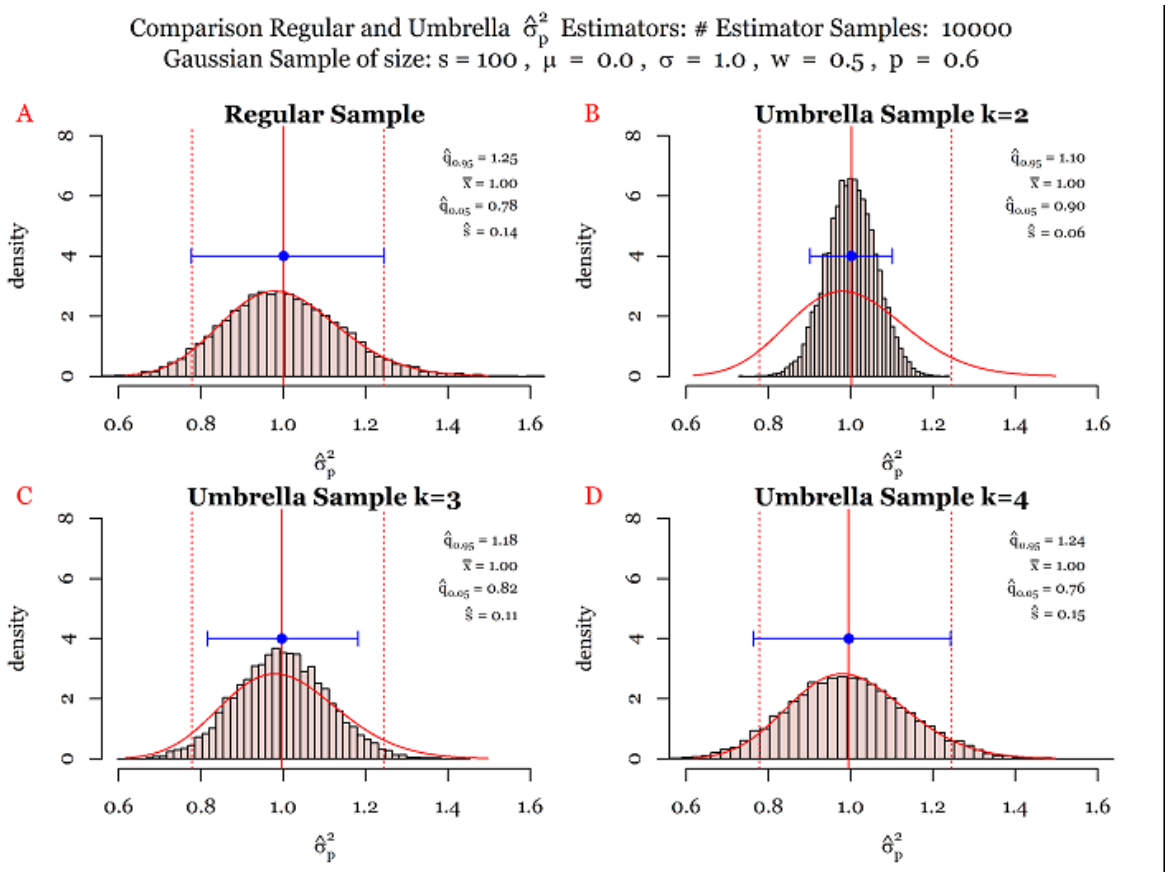


Figure 16. Sampling distributions of variance estimators constructed from samples using regular (A) and umbrella (B–D) non-stratified samples , . A: ; B–D: , for .

The estimator performance in these figures contrasts sharply with the performance of the variance estimator in Figure 6B, where one observed not only a biased estimate for the variance using a sample size of , but also a sample variance of the estimator equal to , which is unacceptable for practical purposes. When contrasting that value of to the values , , in Figure 16B–D, respectively, it is fair to say that a remarkable improvement has been achieved both in terms of the variance of the umbrella estimators for , but also in terms of their sample mean being approximately equal to the variance of the target density .

# 7. MULTIVARIATE UMBRELLA/MIXTURE SAMPLING

The steps to construct a multivariate umbrella pdf for the purpose of umbrella importance sampling are the same as those steps followed for the construction of the univariate umbrella pdf in Section 6. First, a multivariate gamma distribution is constructed with a specified multivariate mode location and a multivariate tail probability. Next, that multivariate gamma tail pdf is reflected in a multivariate manner to construct gamma distributed tails in all the multivariate hyper-quadrants; finally, the multivariate tails distribution is mixed with the multivariate normal distribution to allow for multivariate defensive mixture sampling.

## 7.1 Construction of a Multivariate Gamma Tail pdf

To generalize the construction from a univariate umbrella pdf to a multivariate one, a bivariate gamma pdf is constructed with a mode at  and an origin at . That bivariate gamma pdf is obtained by taking the product of univariate gamma densities

(32)

with a mode at )/ for  and a variance equal to /. Gamma density  follows from  by using an additional horizontal shift-parameter . A bivariate or multivariate density constructed from a product of marginal densities implies statistical independence of its random variables. Because the bivariate (or multivariate) gamma pdf's purpose is to sample in the tails of a multivariate normal distribution, in an umbrella sampling context, this is not considered a restriction. The multivariate normal pdf exhibits tail independence (see, e.g., [21]). The  and  parameters in  are solved for by setting the location of the mode equal to  and the probability mass to the right of the mode , equal to . The procedure to obtain these  and  parameters is analogous to the procedure described in Section 6.1, except that one sets in the procedure in Section 6.1 the location of the mode equal to .

Figure 17A plots such a bivariate gamma pdf with parameters  and  in the positive quadrant. Figure 17B plots the bivariate gamma cdf with the same parameters. The facet panels in Figure 17 plot marginal pdfs and marginal cdfs of the univariate gamma distribution  in red. Because , the gamma pdf plotted in Figure 17A is identical to the one plotted in red in Figure 9B with a mode at  and a mode-exceedance probability . The facets in Figure 17 plot vertically the location of the -axis and the location of the gamma mode. In the -plane, the  and -axis are plotted together with a red -unit square, with vertices/corner points  and  for future reference. Contour lines are plotted in the -plane for the pdf in Figure 17A and for the cdf in Figure 17B. Finally, the vertical facets in Figure 17B plot horizontal lines at  and . The intersection of the horizontal line  and the vertical line  locate the point of inflection of the marginal cdf and, thus, the pdf-mode at .

From the independence of the marginal distributions, it follows that the probability in the -unit square equals , where  is the dimension of the multivariate gamma–tail-distribution construction. Thus, the multivariate exceedance probability equals  since . In other words, as the dimension increases, the exceedance probability increases, keeping the tail probability parameter  fixed.

Figure 18 is analogous to Figure 17, except that the origin of the marginal gamma densities is set at . While the bivariate distribution in Figure 17 and Figure 18 have in common that , one observes from Figure 18 that the effect of moving the origin of the gamma density  to  while keeping  and  fixed, results in a heavier tailed bivariate pdf than the one in Figure 17. In other words, both the exceedance probability parameter  and the origin parameter  drive the heaviness of the tails in Figure 17 and Figure 18.

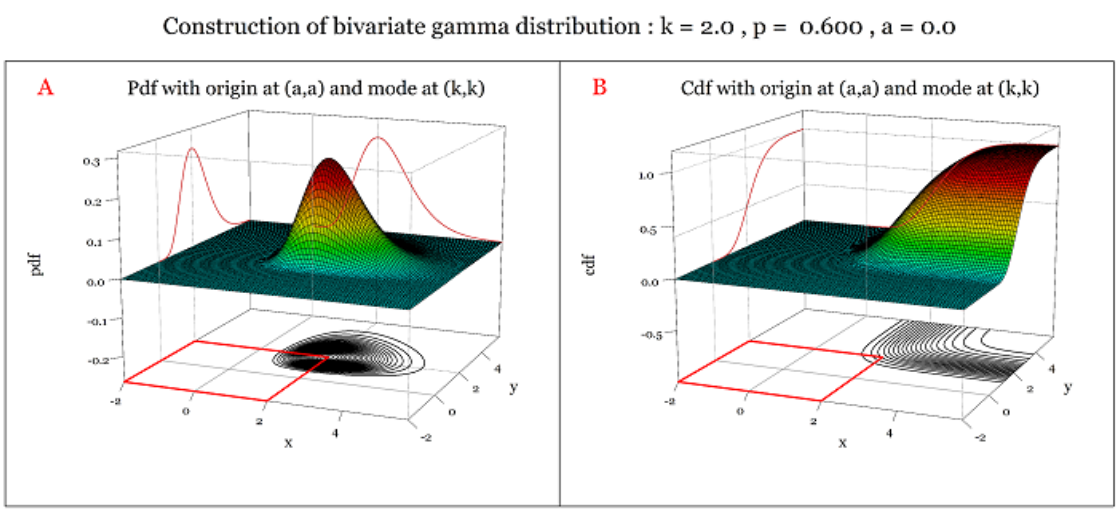


Figure 17. Construction of a bivariate distribution with independent gamma-distributed marginals with a mode at , origin at , and a mode-exceedance probability . A: Bivariate pdf; B: Bivariate cdf.

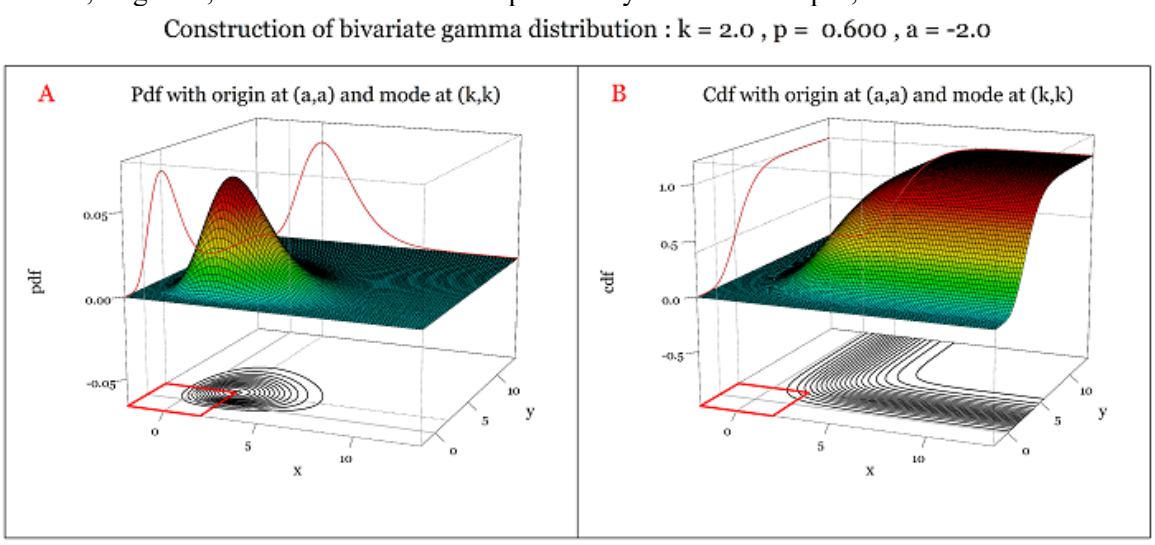


Figure 18. Construction of a bivariate distribution with independent gamma distributed marginals with a mode at , origin at , and a mode-exceedance probability . A: Bivariate pdf; B: Bivariate cdf.

## 7.2 Construction of a Multivariate pdf with Gamma Tails

To construct a bivariate pdf with a gamma-shaped tail at all corner-vertex points , , and of the red k-unit square in Figure 17 or Figure 18, one reflects the gamma pdfs in Figure 17A or Figure 18A in (1) the -axis, (2) the -axis, and (3) the origin . Next, one constructs a mixture of these four bivariate pdfs to obtain a pdf with gamma-shaped tails in all four quadrants of the -plane. By default, an equally weighted mixture of gamma tails with modes at the vertices and is suggested. That being said, non-equal weighting of these gamma tails can be accommodated should one prefer to sample more in one quadrant or another. Figure 19A depicts that construction method utilizing the pdf in Figure 17A under an equal tail-weighting scheme, with every bivariate gamma tail being assigned the mixture-weight . Figure 19B depicts that construction method utilizing the pdf in Figure 17A under an non-equal tail weighting scheme.

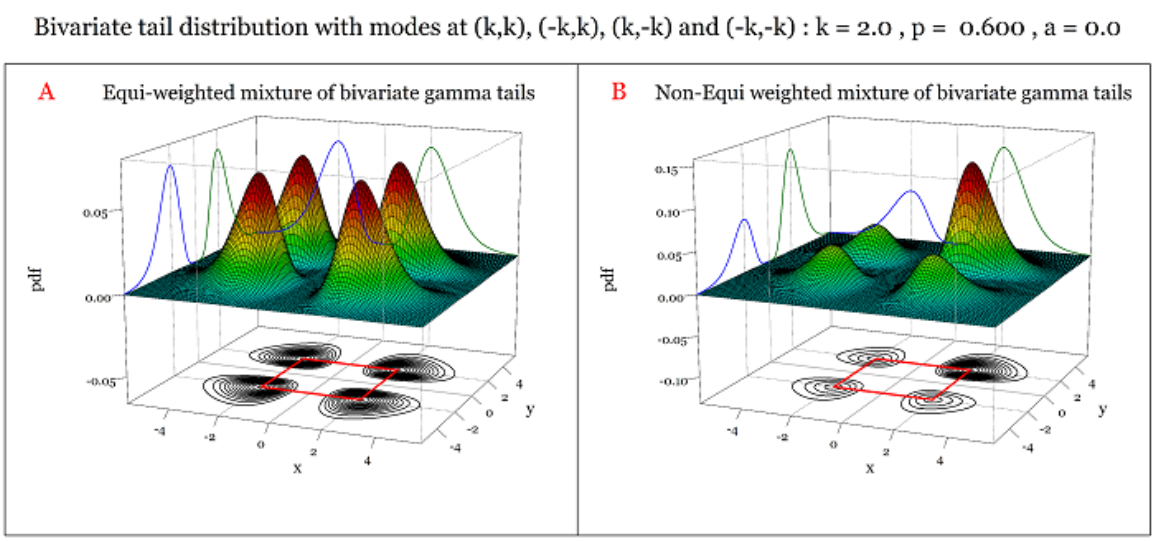


Figure 19. Construction of a bivariate tail distribution with modes at the vertices and . A: Equally weighted mixture of bivariate gamma tails with weights ; B: Nonequally weighted mixture of bivariate gamma tails with weights and .

The mixture-weight of the bivariate gamma pdf in the upper-quadrant is set in Figure 19B equal to . The bivariate gamma pdfs in the other three quadrants are assigned the mixture-weights . Hence, when sampling from the bivariate pdf in 19B, about half of the samples will be drawn from the upper quadrant, and the other half of the samples will be equally distributed over the other three quadrants. The latter thus allows for targeted-sampling of a particular quadrant that should be desirable.

From a marginal distribution perspective, depicted in the facets of Figure 19B, about of those samples are positive valued, and of those samples are negative valued. These probabilities follow immediately from the tail-mixture weights and the fact that the origin parameter in Figure 19B. Naturally, in Figure 19A, about half of the samples are positively valued from a marginal-sampling perspective. A potential drawback of setting the origin parameter in Figure 19 is the prevalence of a low-probability mass distribution at the vicinity of and -axis.

Figure 20 is analogous to Figure 19, except that the mode and origin parameters are set at and , respectively. One thus observes a larger probability mass distributed in the vicinity of the and -axes. Hence, the origin parameter not only drives the heaviness of the tails, but also the probability mass distributed in an axis vicinity. Because of symmetry, it is obvious that about a quarter of samples drawn from the bivariate pdf in Figure 20A are located in each quadrant, and the evaluation of the number of samples drawn in each quadrant in Figure 20B requires the evaluation of the bivariate cumulative distribution function. For example, for the pdf in Figure 20B, one obtains that the upper-quadrant probability equals .

To generalize the construction of the bivariate tails pdf to a multivariate one with a gamma tail in each of the hyper-quadrants, where is the dimension of the multivariate distribution, the same reflection procedure is used as in the construction of Figure 19 and Figure 20.

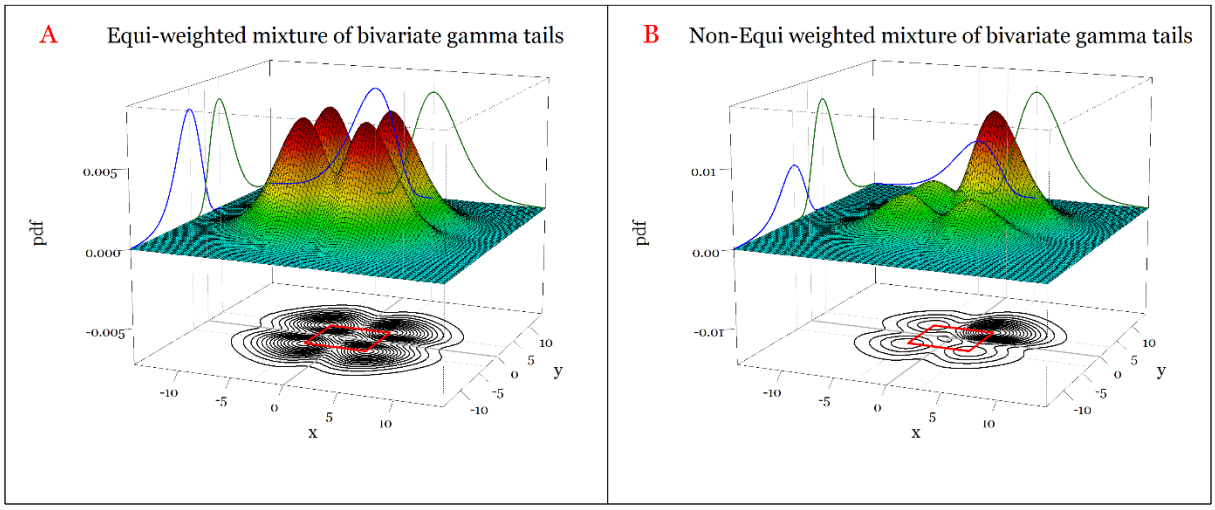


Figure 20. Construction of a bivariate tail distribution with modes at the vertices and . A: Equally weighted mixture of bivariate gamma tails with weights ; B: Nonequally weighted mixture of bivariate gamma tails with weights and .

## 7.3 Construction of a Multivariate Umbrella pdf

The final step in the construction of the multivariate umbrella pdf is the mixing of the original target density with the multivariate gamma tail pdfs, of which the bivariate pdfs displayed in Figure 19 and Figure 20 are examples. Denoting the weight of the target density , the weight of the multivariate gamma tails pdfs equals . Setting the target density equal to a bivariate normal density with correlation and , Figure 21 plots the bivariate umbrella pdfs associated with the gamma-tail distributions plotted in Figure 19. The univariate umbrella pdf plotted in the facets of Figure 21A is identical to the one plotted in Figure 11B. The univariate umbrella pdf plotted in the facets of Figure 21B is a generalization of the univariate umbrella pdf with a higher weight assigned to the right tail. The weights of the univariate target density in Figure 21B equals =0.5 whereas the weight of the left tail equals and of the right tail equals .

Figure 22 plots the bivariate umbrella pdfs associated with gamma-tail distributions in Figure 20. Note that the bivariate gamma-tail distributions, as a mixture member in Figure 22, are less pronounced despite their also being assigned a mixture weight of . This is a result of the bivariate gamma-tail distributions in Figure 20 being more heavily tailed than the tails distribution in Figure 19. That being said, the gamma univariate tails in the facets of Figure 22 are more pronounced as a result of probability mass being accumulated in either the or -direction when evaluating these marginal umbrella pdfs in Figure 22. Observe from Figure 22B that the right tail of that univariate umbrella pdf is heavier than the left tail. The weights for each of the mixture members in the univariate umbrella pdf in Figure 22 are the same as those as in Figure 21. The only difference in the construction of Figure 21 and Figure 22 is that the mode parameter and the origin parameter in Figure 22 equal and while those in Figure 21 equal and .

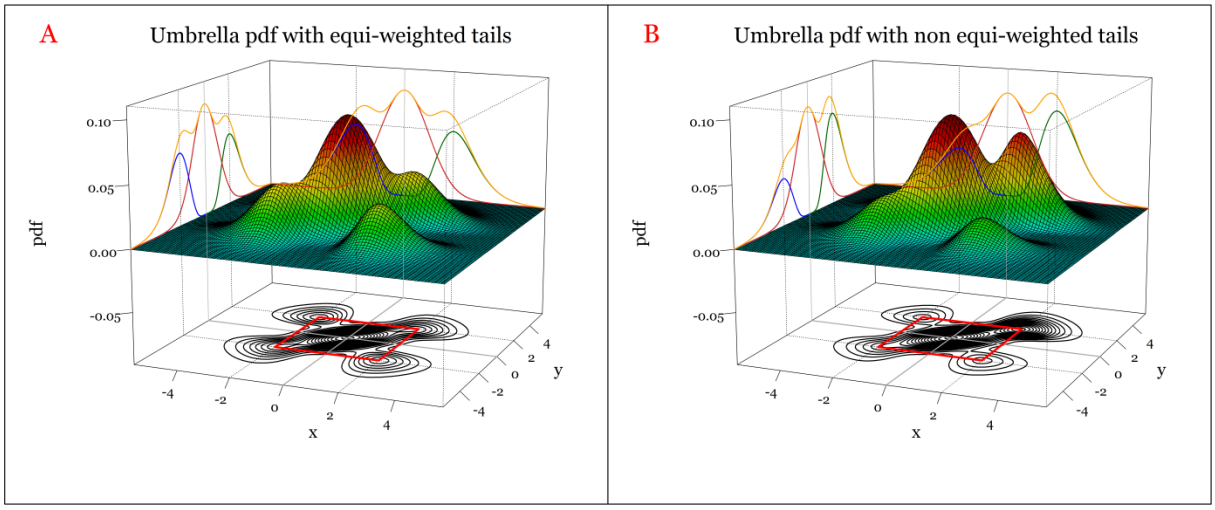


Figure 21. Construction of a bivariate umbrella pdf as a mixture of a bivariate normal (BVN) distribution with correlation and bivariate tails distribution. A: BVN pdf mixed with bivariate tails pdf from Figure 19A; B: BVN pdf mixed with bivariate tails pdf from Figure 19B.

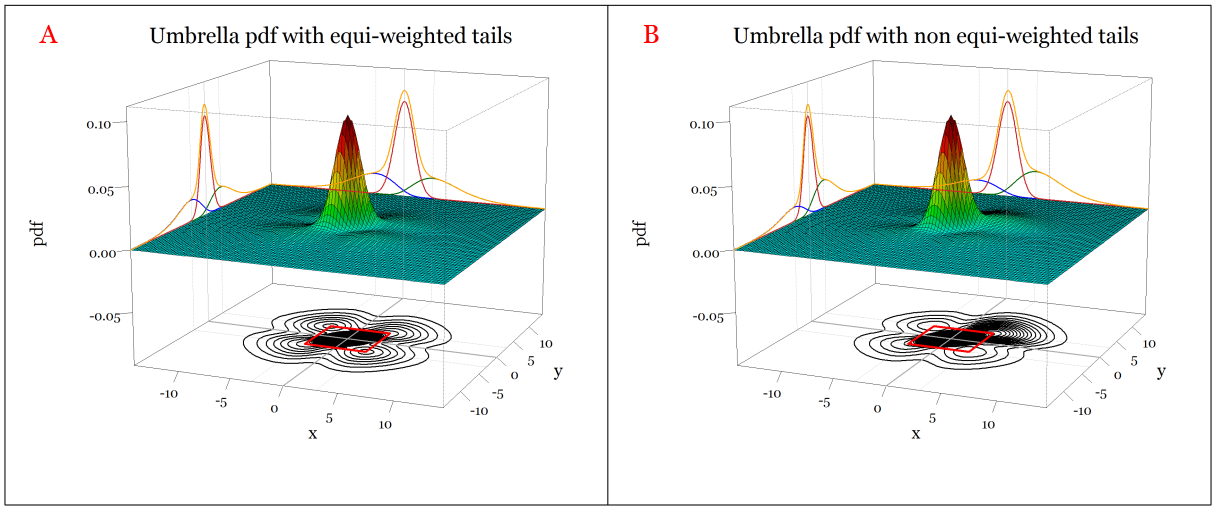


Figure 22. Construction of a bivariate umbrella pdf as a mixture of a BVN distribution with correlation and bivariate tails distribution. A: BVN pdf mixed with bivariate tails pdf from Figure 20A; B: BVN pdf mixed with bivariate tails pdf from Figure 20B.

## 7.4 **Sampling from a Multivariate Umbrella pdf**

To construct an umbrella sample of size , one first generates a sample of of size from a Bernoulli(π) distribution with . Using that Bernoulli sample, one evaluates the number of samples to be drawn from the target density . Next, a sample of size is generated from the multivariate distribution with gamma tails, as per the construction in Section 7.2. To generate such a sample, one first generates a sample of size from a multivariate gamma tail distribution constructed in Section 7.1 with its tail in the positive hyper-quadrant. For example, in Figure 23, samples are split into samples from the target density (plotted in Figure 23A) and samples from a bivariate gamma pdf (plotted in Figure 23B) similar to the one plotted in Figure 17, except that in Figure 23B the mode parameter .

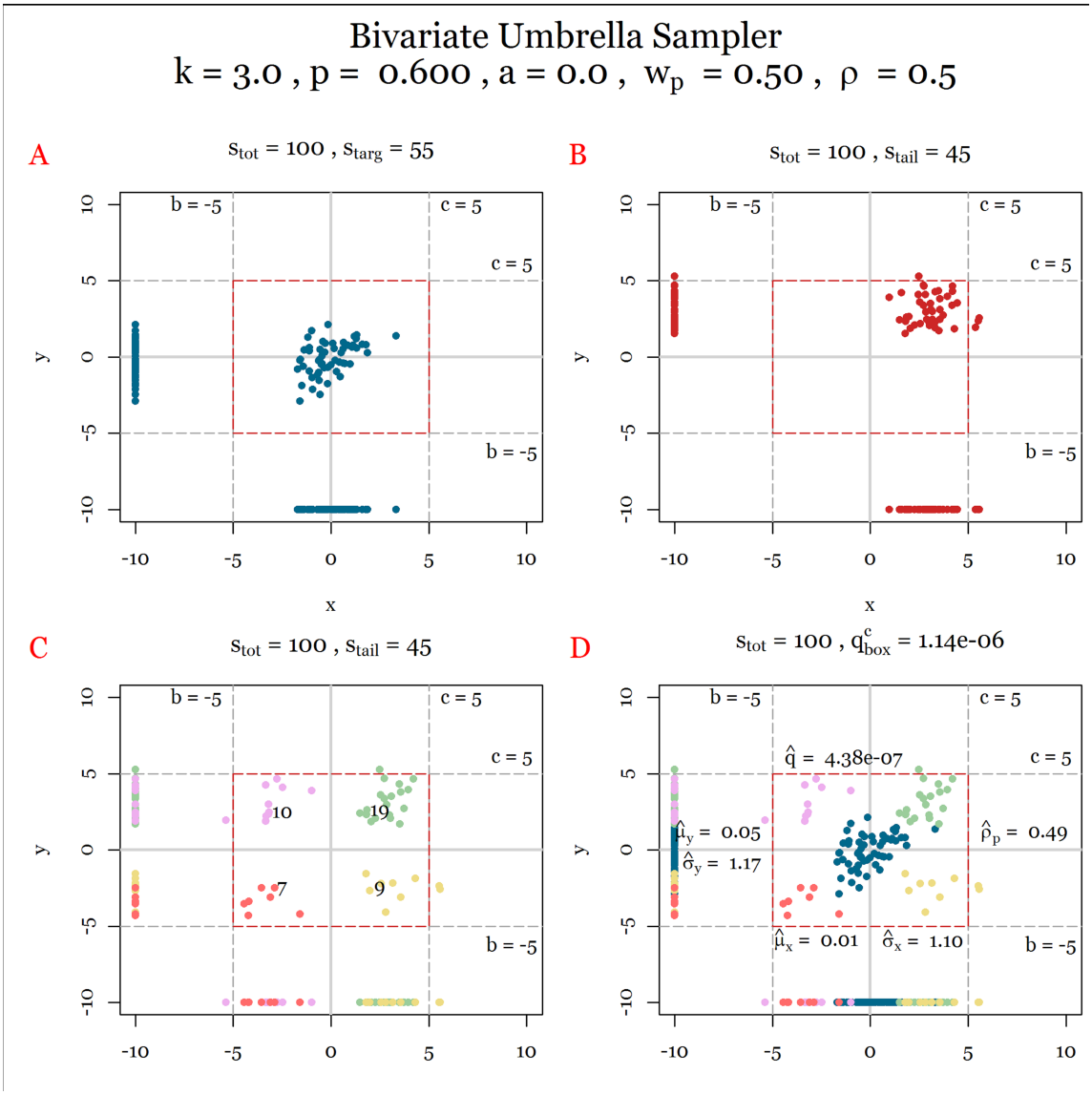


Figure 23. Construction of a bivariate umbrella sample of size with equal-weighted gamma tails. A: Sample of size from BVN distribution with correlation ; B: Sample of size from a bivariate gamma tail distribution similar to Figure 17; Sample of size from a bivariate multi-tail distribution similar to Figure 19A; Sample of size from a bivariate umbrella distribution similar to Figure 21A.

Next, one generates a sample of size  from a discrete distribution with probability-mass function , where  are the weights of the mixture distribution of gamma tails as per the construction in Section 7.2. Denoting the latter a vertex selection sample, the sample from the multivariate gamma-tail distribution in the positive hyper-quadrant is transformed into a sample from the different gamma tails with their modes at the vertices of the -dimensional hypercube. For example, to transform a sample from the bivariate gamma-tail distribution with a mode at  to a sample of a bivariate gamma-tail distribution with a mode at , one multiplies both the -coordinate and -coordinate by . The  samples in Figure 23B are split in this manner in Figure 23C using a uniform pmf with outcomes  into , , , and  samples in the first, second, third, and fourth quadrant, respectively. Thus, the sample plotted in Figure 23C is a sample of size  from a bivariate gamma-tails distribution similar to the one in Figure 19A except that, in Figure 23C, the mode parameter . Finally, the samples in Figure 23A and Figure 23C are combined into the umbrella sample of size  plotted in Figure 23D.

In Figure 23, a red square is plotted with coordinates , , , . The coverage probability of the bivariare normal distribution inside this red box equals . In other words, nearly all the probability mass of the target density  is contained within this red square. One observes from Figure 23A that none of the  samples fall outside this red box (as expected).

The probability coverage of the target density outside of this red box equals , and its value is plotted in the subtitle of Figure 23D. One observes from Figure 23B and Figure 23C that at least three samples fall outside this red box. These are used to estimate the “out-of-box” probability  plotted above the red box in 23D, as per the importance-sample estimation procedure discussed in Section 4. The importance estimates for the means and standard deviations of the marginals of the standard bivariate normal distribution with Pearson’s product moment correlation  are displayed in Figure 23D, together with the importance estimate  for that product-moment correlation.

Figure 24 was constructed in the same manner as Figure 23, except that, in Figure 24, a sample was generated from the bivariate distribution in Figure 20A with heavier tails than the bivariate distribution in 19A. Comparing Figure 23C with Figure 24C, one observes more sample outside the red box in Figure 24C to estimate . The “out-of-box” probability  is estimated in Figure 24D at , and the Pearson product moment correlation is also estimated, at .

Figure 25 demonstrates the four extreme scenarios of umbrella sampling with unequal weighted gamma tails, with Figure 25A–D having a single bivariate gamma-tail sample in the first, second, third and fourth quadrant, respectively.

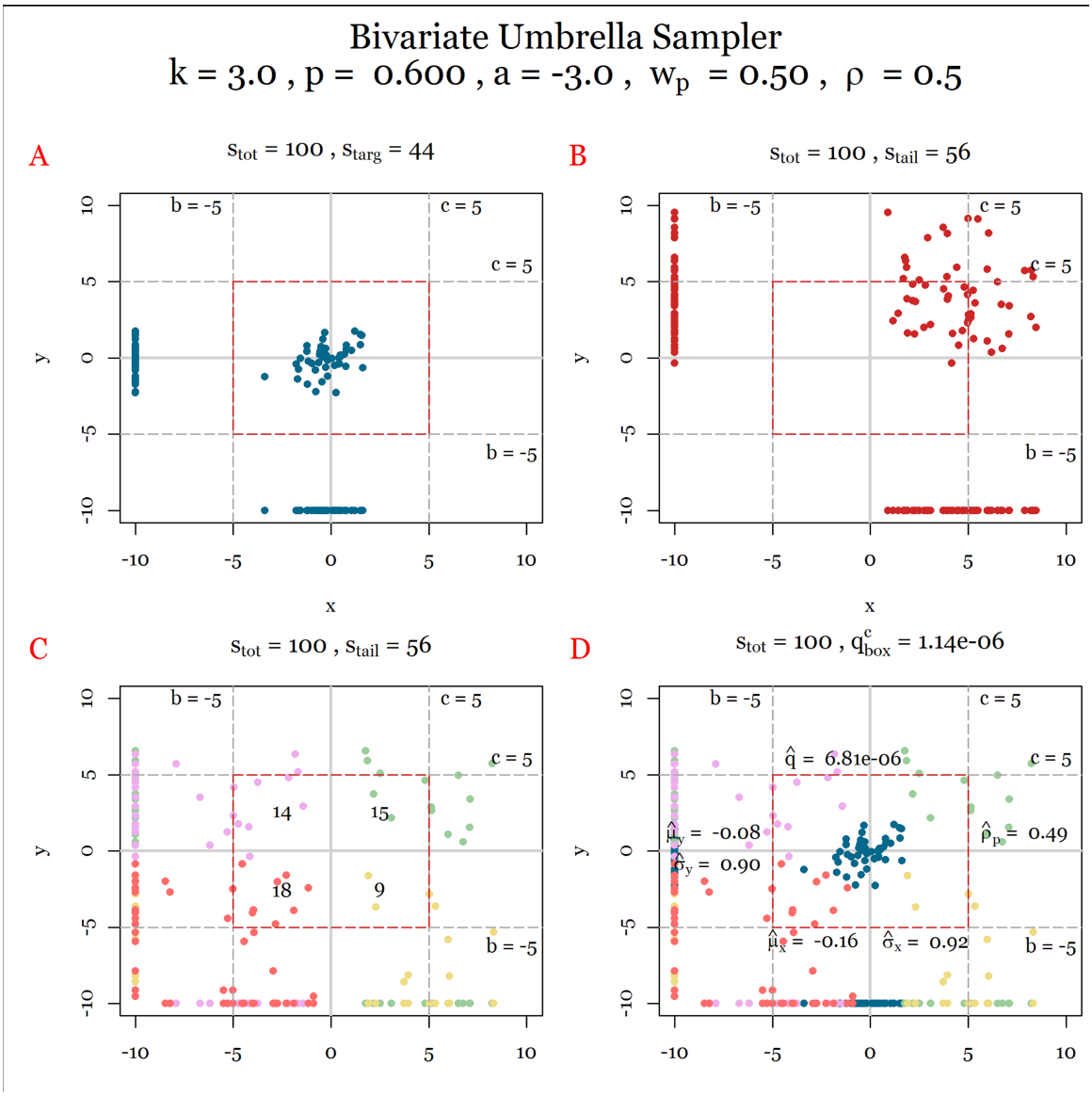


Figure 24. Construction of a bivariate umbrella sample of size , with equal-weighted gamma tails. A: Sample of size from BVN distribution with correlation ; B: Sample of size from bivariate distribution in Figure 18; Sample of size from bivariate distribution in Figure 20A; Sample of size from bivariate umbrella distribution in Figure 22A.

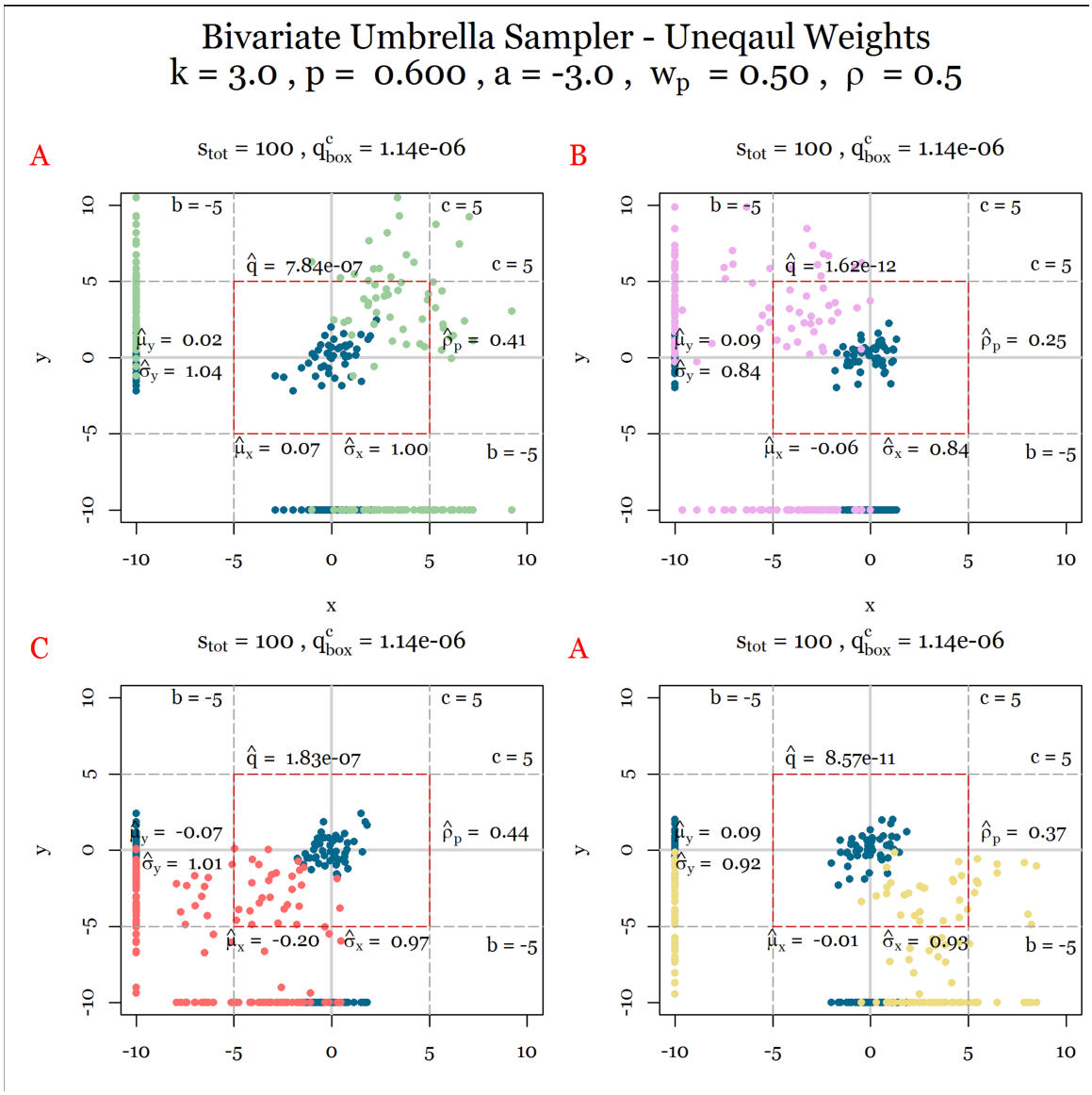


Figure 25. Examples a bivariate umbrella sample of size , with unequal-weighted tails and a BVN distribution, with correlation . A: Umbrella sample with the first quadrant gamma tail; B: Umbrella sample with second quadrant gamma tail; C: Umbrella sample with third quadrant gamma tail; D: Umbrella sample with fourth quadrant gamma tail.

## 7.5 Bivariate Umbrella Estimator Behavior

In this section the performance of the correlation estimator and out-of-box probability estimator in Figure 23–Figure 25 will be studied under regular and umbrella sampling. The classical estimator for the Pearson product moment correlation under regular sampling is given by

(33)

where

(34)

and

(35)

The theoretical sampling distribution of the estimator for the case that are bivariate normal distributed with correlation coefficient was obtained by [22], but is very complex. The mean and the variance of the estimator are given by [23],

(36)

In other words, is a biased estimator for the correlation coefficient , provided , with a negative bias when and a positive one when .

For practical purposes, [24] demonstrated that the sampling distribution of can be well approximated in that case using

(37)

where

(38)

From and , one obtains of the approximating density for the estimator

(39)

Figure 26 plots the pdf in red. The solid vertical lines in red are plotted at . The dashed vertical lines in Figure 26 are plotted at the theoretical and percentiles of .

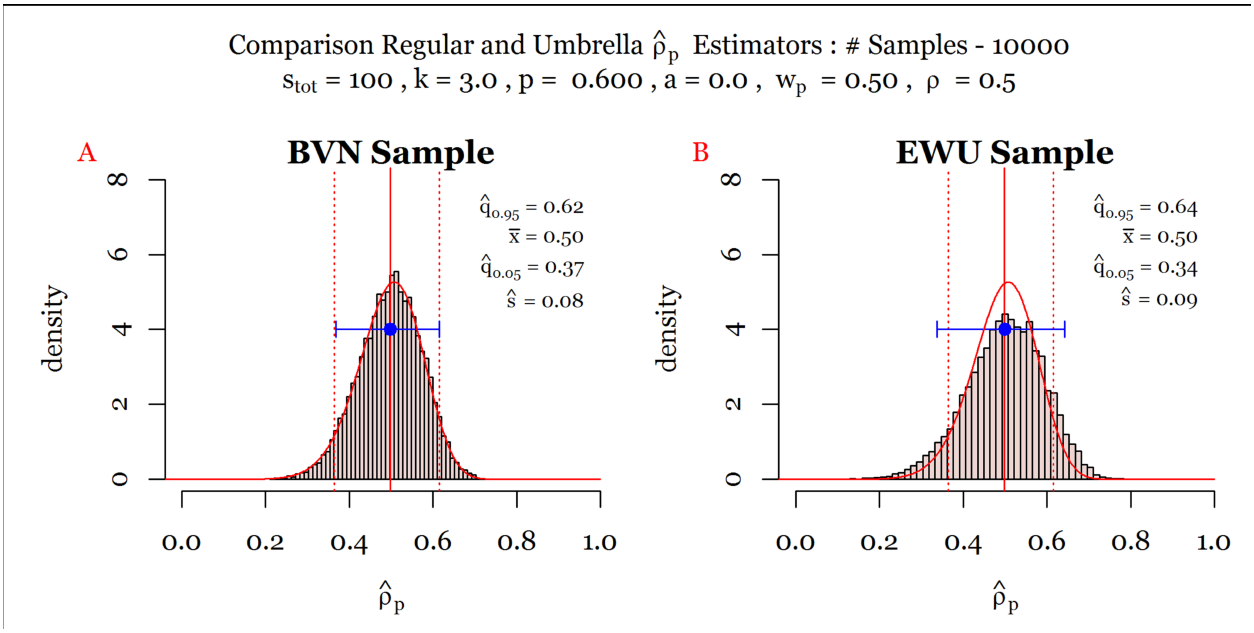


Figure 26. Sampling distributions for correlation estimators constructed from samples using regular (A) and umbrella (B) non-stratified samples , . A: Sampling distribution of , with ; B: Sampling distribution of umbrella estimator using the equally weighted umbrella () pdf in Figure 21A.

The empirical sampling distribution plotted in Figure 26A was estimated under regular sampling using samples of size from a BVN with and standard normal marginal distributions. One observes a close match between the pdf and the empirically estimated density in Figure 26A. The error bar end points, in blue in Figure 26A, are the empirical and percentiles estimated from the regular samples. Here too, one observes a close match in Figure 26A.

Figure 26B plots the empirical sampling distribution of the umbrella estimator  for the correlation coefficient. It was estimated under umbrella sampling using  samples of size  from the equally weighted umbrella (EWU) pdf in in Figure 21A. One observes from Figure 26B an increase in the standard deviation of that sampling distribution and a widening of the blue error bar in Figure 26B with the empirical  and  percentiles as its end points. That being said, the difference between the empirical sampling distribution in Figure 26B compared to the pdf  can be considered marginal.

Figure 27 is analogous to Figure 26, except that the sampling distribution of the umbrella estimator in Figure 27B was generated using the umbrella pdf in Figure 22A with mode parameter  and origin parameter .

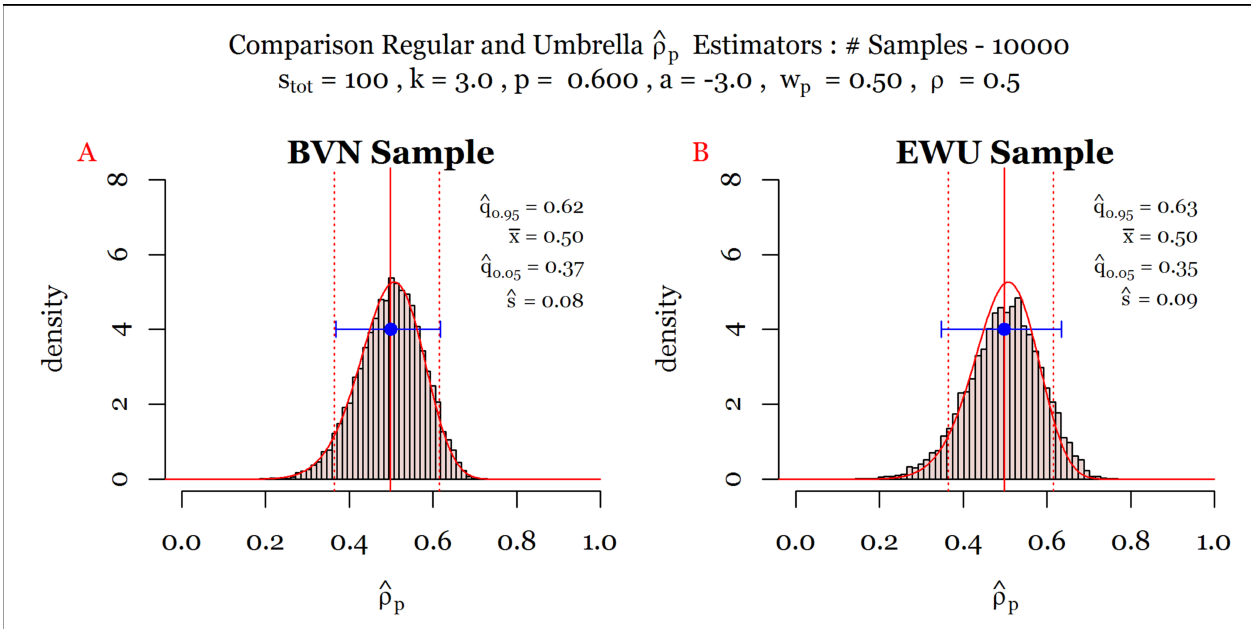


Figure 27. Sampling distributions for correlation estimators constructed from  samples using regular (A) and umbrella (B) non-stratified samples , . A: Sampling distribution of  ,  with ; B: Sampling distribution of umbrella estimator  using the EWU pdf in Figure 22A.

These parameter settings not only result in heavier tails, as displayed in Figure 22A, than in Figure 21A, but also have a higher probability mass distributed in the vicinity of the axes, as exemplified by comparing Figure 19A to Figure 20A. When comparing Figure 27B to Figure 26B, one observes a minor improvement in the empirical umbrella estimator distribution for  in Figure 27B, which perhaps can be attributed to the origin parameter  in Figure 27B, as opposed to the origin parameter  in Figure 26B, and not to the larger number of samples outside the red box when comparing Figure 23 to Figure 24. Indeed, a larger number of samples is observed outside the red box in Figure 24 than in in Figure 23, but these samples are assigned a lesser importance weight in the umbrella estimation procedure for  than the samples inside the red box in Figure 24.

Figure 28 too is analogous to Figure 26, except that the empirical sampling distribution for the umbrella estimator  in Figure 28A–D were generated from the nonequally weighted umbrella (NEWU) pdfs used to generate the umbrella samples in Figure 25A–D, with mode parameter  and origin parameter .

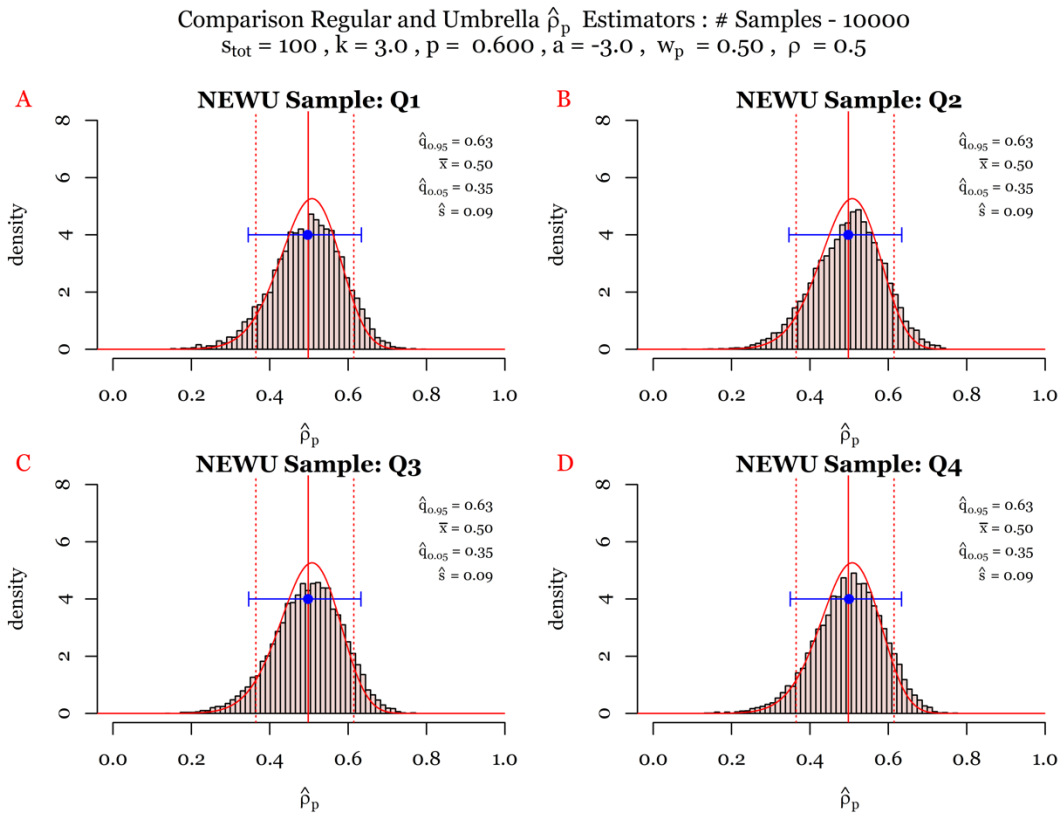


Figure 28. Sampling distributions for correlation umbrella estimators constructed from samples using umbrella non-stratified samples , , from the (NEWU) pdfs in Figure 25A–D. A: First-quadrant NEWU sampling; B: Second-quadrant NEWU sampling; C: Third-quadrant NEWU sampling; D: Fourth-quadrant NEWU sampling.

Comparing the empirical-sampling distributions in Figure 28 to the empirical-sampling distribution in Figure 27D, one observes no reduction in performance as a result of utilizing a NEWU sampling scheme. The latter is perhaps surprising, given that a reduction in performance of importance variance estimators was demonstrated using an importance density weighted towards a single tail in Section 5. Perhaps that reduction in performance is not observed in Figure 28 because the estimators of , and given by and are statistically dependent. Barring a specific reason to steer an umbrella-sampling procedure towards a particular hyper-quadrant, it is recommended that—due to the reduction in performance, in particular of the importance-variance estimators weighted towards a single tails demonstrated in Section 5—an EWU sampling procedure be used.

Finally, Figure 29 plots the empirical-sampling distribution for the out-of-box probability estimator for constructed from estimator samples obtained using umbrella non-stratified samples , , from the EWU pdf in Figure 22A. Umbrella sampling from that pdf was demonstrated in Figure 24.

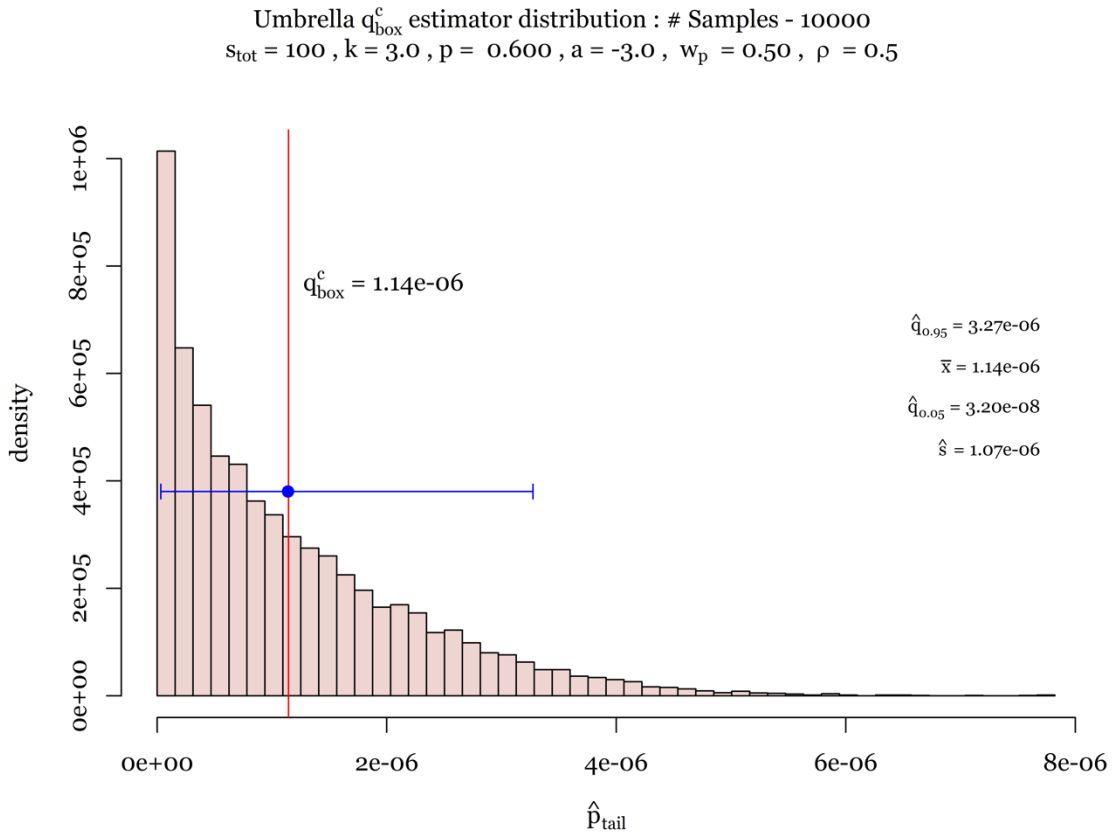


Figure 29. Empirical sampling distribution for the out-of-box probability estimator for constructed from estimator samples obtained using umbrella non-stratified samples , , from the EWU pdf in Figure 22A. Umbrella sampling from that pdf was demonstrated in Figure 24.

The out-of-box probability was evaluated for a BVN distribution with standard normal marginal distributions and a correlation in Figure 24. The box was plotted as a red square in Figure 24, with coordinates , , , . One observes that the estimated mean of the umbrella-sampling distribution depicted in Figure 29 coincides with the value . It is important to note here that the probabilities estimated using umbrella sampling were obtained using only samples. Under regular sampling from a BVN distribution with standard normal marginals, zero out-of-box probabilities were estimated in all estimates for this probability using samples. This is to be expected because the coverage probability inside the red box of that BVN distribution equals . The blue error bar in Figure 29 plots the empirically estimated 5th and 95th percentile evaluated at and , respectively. The standard deviation of the empirical-estimator distribution is evaluated as , resulting in a coefficient of variation estimate equal to , which is about twice the coefficient of variation in Figure 14E, but in the same order of magnitude. It should be noted, however, that the coefficient of variation in 14E was estimated for the univariate probability as opposed to the bivariate out-of-box probability , which perhaps explains the reduction in performance for the coefficient of variation in Figure 29.

# 8. ENGINEERING UNCERTAINTY-ANALYSIS EXAMPLE

In this section, the umbrella-sampling procedure is demonstrated to estimate tail probabilities in an illustrative engineering-uncertainty analysis case [25]. This case involves the Stephan-Boltzman equation for radiation. An occurrence in nature is how two objects in contact arrive at thermal equilibrium because heat flows from the higher-temperature to the lower-temperature object until they are both in equilibrium. Even when the objects are not in contact or there is no physical medium between them, thermal equilibrium is still achieved through electromagnetic radiation, and the emitted energy is referred to as black-body or thermal radiation. It has been found that the amount of radiation emitted is proportional to the temperature of the object. In fact, the law that describes this relationship was first experimentally discovered by Josef Stefan and, shortly after, Ludwig Boltzmann, who derived it theoretically [26].

While the Stefan-Boltzmann law has obvious terrestrial applications, it also has a great deal of importance to energy engineering. For example, measuring the actual physical properties of nuclear fusion or fission processes is herculean if not impossible. Nonetheless, by observing the black-body radiation spectrum, estimating the reaction temperature and energy output of a nuclear process are possible. Planck's law models a spectrum of this radiation as a function of wavelengths [27], the integral of which is the Stefan-Boltmann Law.

Though the obvious application of the Stefan-Boltzmann law is in the measurement of the amount of heat radiated from a black body, it readily finds applications in contexts in which the conversion of temperature is required to determine the intensity or power per unit-area intensity. Take, for example, the Systems for Nuclear Auxiliary Power (SNAP-1) program that used the heat from a decaying radioisotope, cerium-144 to generate 500 W of electrical power. SNAP-2 was designed as a reactor-heated electrical power plant to produce 3 kW, and further advances led to the development of a 35 kW power plant and the fission battery in SNAP-10 [28]. The limitations of nuclear systems to power space explorations during extensive orbiting in dark areas led to the use of solar cells and batteries for power. Thus, the inherent advantages of the ability to harness electrical power from radiation are not only readily useful for fission processes, but also for solar photovoltaic energy generation.

The Stefan-Boltzmann equation is given by

(40)

where  is the sample emissivity,  is the energy transfer rate,  is the cross sectional area of the emitter,  is the view factor,  is the Stephan-Boltzmann constant,  is the radius of the emitter,  is the dimension of the square sample area, and  and  are the sample and radiometer temperatures, respectively. The following uncertainty information about the input parameters is available from [25] in Table 1.

The objective of the uncertainty analysis is, first, to determine two random tolerance limits,  and , using the two-quantile Wilks method [29] such that the probability that the sample emissivity  falls between these two tolerance limits  and , satisfies

(41)

where ,  and  and  are approximately equal to the  and  quantiles of . Next, realizations  of  are obtained via sampling. Having established those two tolerance limits,  and , one concludes that one is about  certain that

(42)

Using regular sampling for emissivity to establish tolerance limits  and , classic estimates for its mean and standard deviation can be obtained. These are compared to their importance-estimated counterparts obtained via the umbrella estimation procedure, which uses umbrella samples to estimate extreme tail probabilities.

Table 1. Uncertainty information available for the Stephan-Boltzman equation

| Parameter | Value | Error |
|---|---|---|

| | | |
|---|---|---|
| | | |
| | | |
| | | |
| | | |
| | | |

## 8.1 Estimating Emissivity Wilks' Tolerance Limits

Interpreting the error information as six-sigma limits, popularized in the quality control literature (see, e.g., Kubiak and Benbow 2016), one directly obtains the standard errors for the marginal distributions of the input parameters to the Stephan-Boltzman equation . For example, one obtains for the standard error of the value . Per the six-sigma paradigm, normally distributed error distributions are assumed [30].

In the absence of a specified degree of dependence between the marginal distributions, two dependence scenarios are considered. The first scenario assumes that the marginal distributions of the input parameters in the Stephan-Boltzman equation are statistically independent. For the second scenario, a Pearson-correlation matrix is assumed, with product-moment correlations among the input parameters. In both scenarios, the form of the distribution of sample emissivity is unknown, and the two-quantile Wilks' method (see, Van Dorp et al. 2021), demonstrated in Figure 30, is employed. From Figure 30, one concludes that for each dependence scenario, a multivariate sample of size must be generated. For each six-dimensional multivariate sample of the input parameters, the sample emissivity is evaluated as per . Moreover, from the two-quantile Wilks analysis in Figure 30, the tolerance limits to be evaluated are

(43)

In other words, the tolerance limits and are the th and th order-statistics in a sample of emissivity of size .

Table 2 provides a set of tolerance limits obtained in this manner for the two analysis scenarios described above. Hence, for example, one concludes from Table 2 for the independence-uncertainty analysis scenario with that with a % tolerance and confidence coefficient. A similar conclusion can be drawn from the tolerance limits for the other statistical dependence scenario, . Table 2 also provides the classic estimates for mean emissivity and its standard deviation obtained using these samples of size . One evaluates from the sample size, , a combined extreme tail-probability estimate

(44)

where is the minimum emissivity observation in a sample of size , and is the maximum observation. Their values and the combined extreme tail probabilities are provided in Table 2 as well.

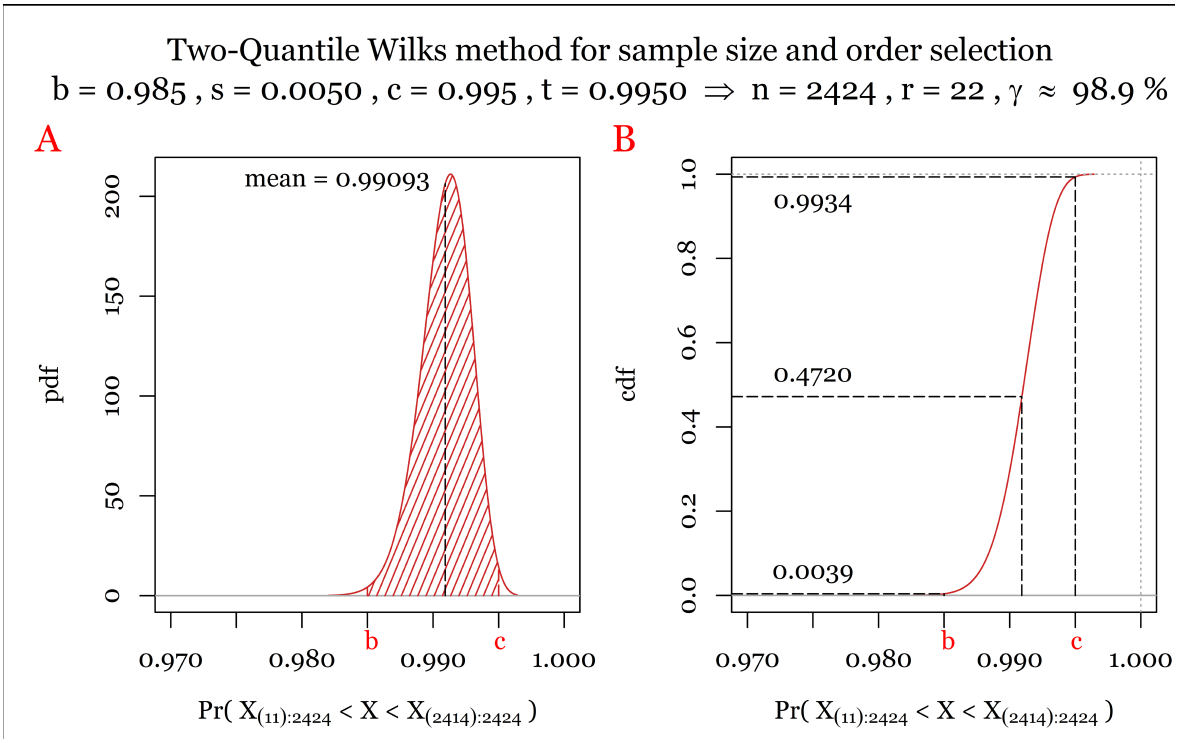


Figure 30. Two-quantile Wilks' analysis demonstration of with %.

Table 2. Two-quantile method Wilks' tolerance limits realizations and mean and standard-deviation estimates that follow from the analysis in Figure 30 for the Stephan-Boltzman equation under two statistical dependence scenarios, given the uncertainty information specified in Table 1.

| Scenario | | |
|---|---|---|
| Tolerance limits | | |
| Mean emissivity | | |
| SD emissivity | | |
| Min emissivity | | |
| Max emissivity | | |
| Extreme tails probability | | |

Naturally, except for the combined tail probabilities, one observes from Table 2 that different tolerance limits, mean values, standard deviation,s and extremes are obtained for each analysis scenario. Figure 31 plots the empirical cumulative distributions (ecdfs) for the two analysis scenarios and .

The tolerance limits in the first row of Table 2 are plotted using vertical dotted lines in the same color as the ecdf in Figure 31. The extremes in the fourth and fifth row of Table 2 are plotted using vertical dashed lines in the same color as the ecdf in Figure 31. One concludes from Figure 31 that the range of the empirical cdf under the statistical independence scenario among the marginal Gaussian distributions is

wider than under the statistical dependence scenario .

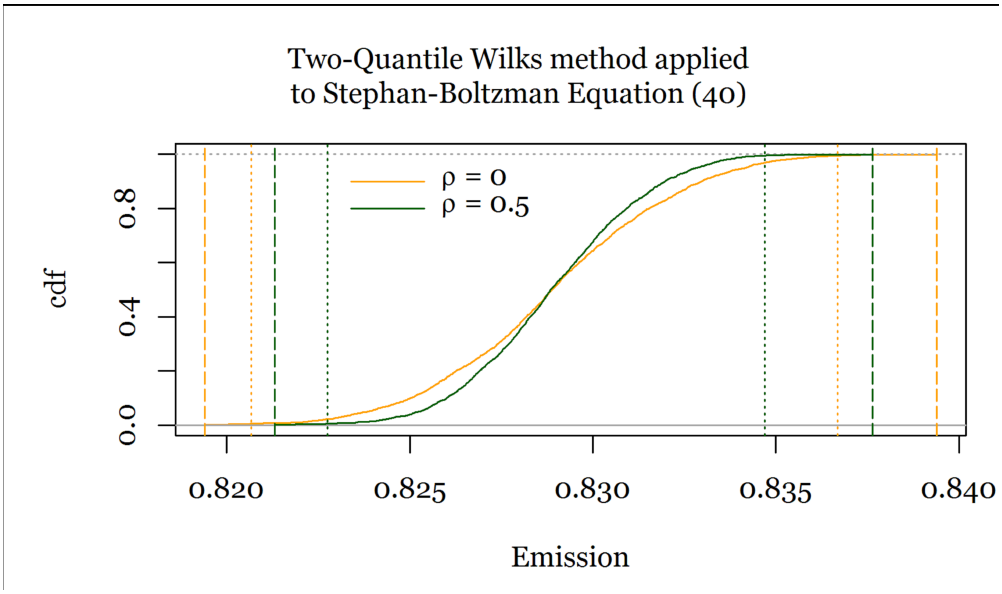


Figure 31. Two-quantile Wilks' analysis demonstration of with %.

## 8.2 Evaluating emissivity uncertainty using umbrella sampling

To sample from a six dimensional multivariate umbrella distribution, the procedure described in Section 7 is used. In that umbrella-sampling procedure, however, the target distribution is a multivariate normal (MVN) distribution with a mean vector at the origin and a given correlation matrix . The MVN distribution in this particular example has mean values and standard deviations as provided in Table 1 thus requiring a scale transformation for both the target MVN pdf and the multivariate umbrella pdf. Because both the umbrella pdf and target distribution in the umbrella-sampling procedure are scaled in the same manner, however, and as a result are multiplied with the same scaling constants, the importance weights , for the umbrella estimation can be obtained using the non-scaled umbrella sampling procedure discussed in Section 7. Summarizing, one first generates an umbrella sample as per Section 7 to obtain the importance weights , and one next transforms for a particular marginal random variable with mean and standard deviation its umbrella sample into a scaled umbrella sample , where

(45)

### 8.2.1 Input variables estimator behavior

One obtains for the mean umbrella estimate of the scaled random variable

(46)

where is the non-scaled random variable. From , it follows that linearity of expectation in the traditional importance-sampling procedure is not preserved when , which is prevalent for, say, a small sample of size , as demonstrated in Figure 2. Under traditional importance sampling, estimation *linearity of expectation* is thus only preserved as per when . As a result, traditional importance-sampling estimation performance may decrease under linear scale transformations, especially when the mean of the transformed random variable is large compared to its standard deviation as is the case, for example, for the variable in Table 2. For this reason, the self-normalized importance sampling procedure [31] is adopted in this example utilizing self-normalized importance weights—i.e.,

(47)

Figure 32 and Figure 33 plot the empirical umbrella mean-estimator distributions for all six input variables in Table 1 for  and , respectively, using self-normalized importance sampling. The solid red lines plot the theoretical estimator distributions under regular sampling (which is a normal distribution). The vertical dashed red lines are plotted at the theoretical th and th percentiles under regular sampling and estimation. The vertical solid dashed lines are plotted at the mean values provided in Table 1. On the other hand, the blue error bars in these figures estimate the th, th empirical percentiles of the mean umbrella estimators together with their empirical-umbrella mean estimate. The mean values of the umbrella estimators of the input variables in Figure 32 and Figure 33 align with the values provided in Table 1. Moreover, one observes a reasonable of the mean umbrella estimators under the linear-scale transformations when comparing the empirical pdfs to the theoretical ones (plotted in solid red) in Figure 32 and Figure 33. A lesser performance is observed for  in Figure 33 than in Figure 32 for .

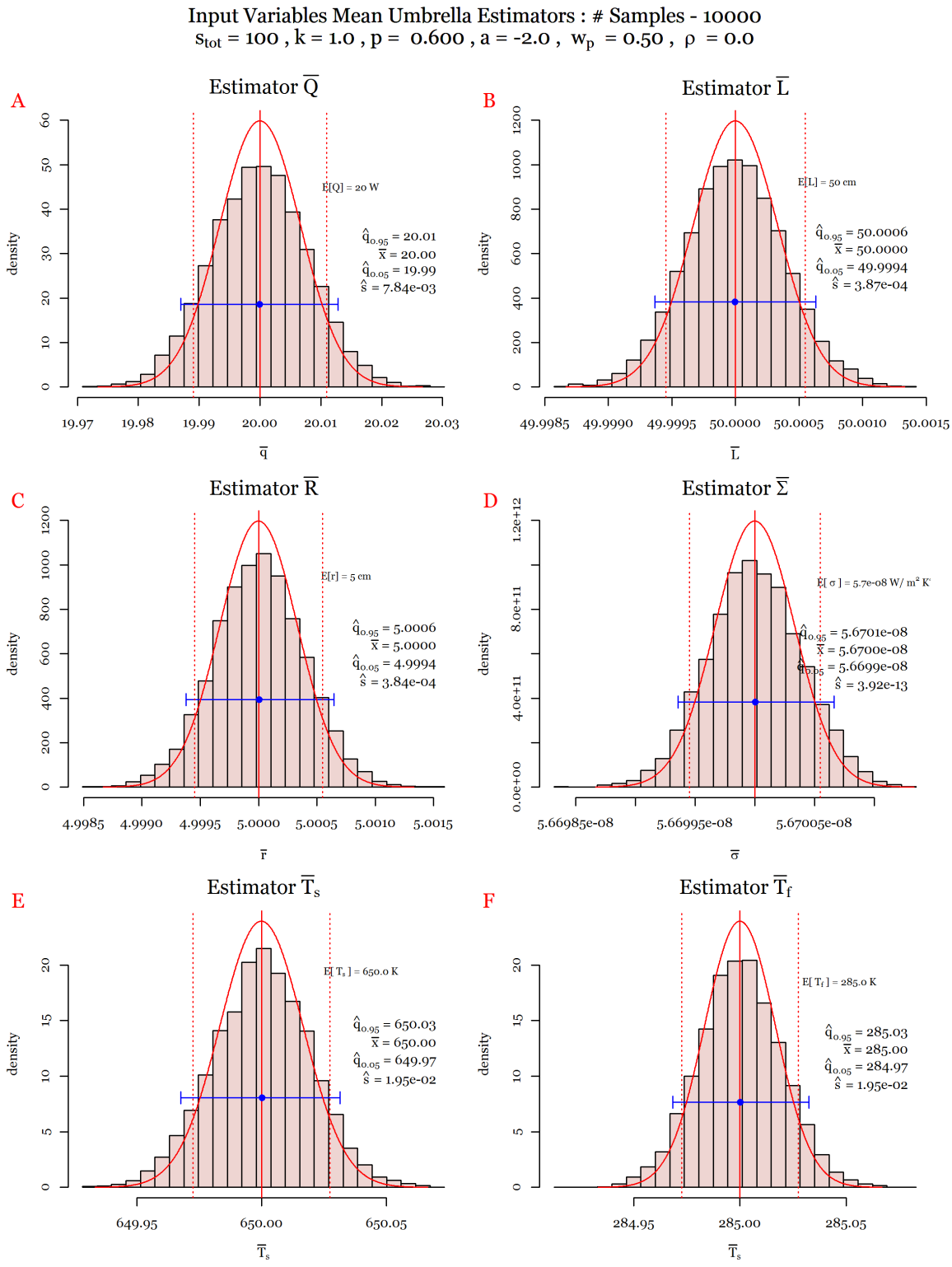


Figure 32. Comparison of theoretical and empirical mean estimator distributions for the input variables in Table 1 under regular sampling and umbrella sampling using self-normalized importance weights for the analysis scenario .

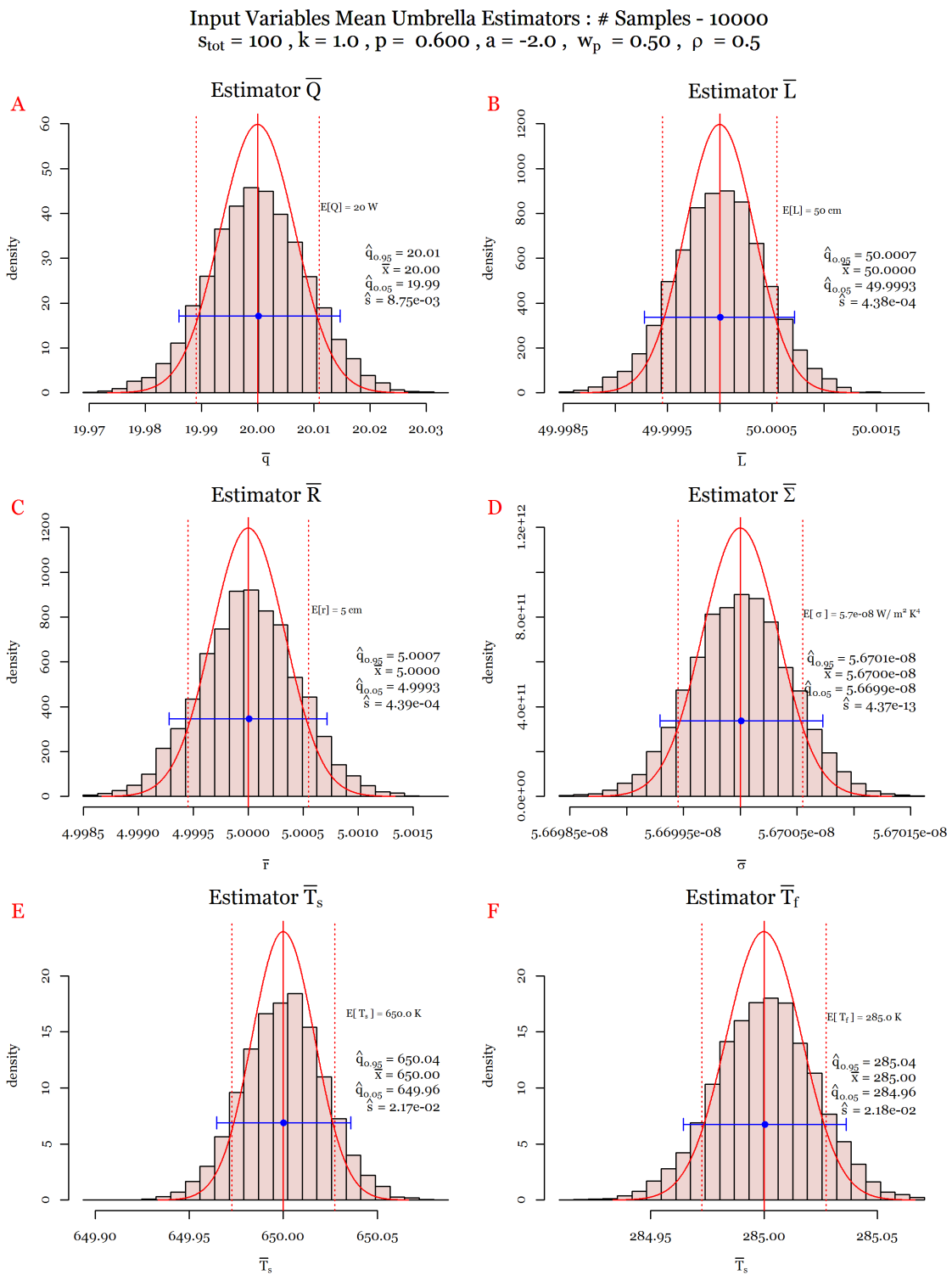


Figure 33. Comparison of theoretical and empirical mean estimator distributions for the input variables in Table 1 under regular sampling and umbrella sampling using self-normalized importance sampling for the analysis scenario .

Figure 34 and Figure 35 are similar to Figure 32 and Figure 33, except that these figures plot the empirical estimator and theoretical estimator distribution for the standard deviation under self-normalized umbrella sampling. The theoretical estimator distribution plotted in red is a transformed  distribution with  degrees of freedom. The vertical solid and dashed red lines plot the theoretical values of the mean for the standard deviation estimator (which is biased) and its theoretical quantiles. The blue error bars plot the empirically estimated counterparts. Similar conclusions can be drawn from Figure 34 and Figure 35 as were drawn from Figure 32 and Figure 33. That is, the empirical mean values of the standard-deviation umbrella estimators under self-normalized importance samples align with the six-sigma standard deviations (plotted using a solid vertical red line) that follow from Table 1 as described in the first paragraph of Section 8.1. Moreover, the empirical quantiles align reasonably well with the theoretical ones obtained under regular sampling. As is the case in Figure 32 and Figure 33, a lesser performance is observed for the estimators in Figure 35 for the case  than for the estimators in Figure 34 for  by comparing the theoretical estimator distribution under regular sampling in (plotted in a solid red line in Figure 34 and Figure 35) to the estimated empirical density functions (plotted as histograms).

Because all paired random variables in Table 1 were assigned the same correlation  for the statistical-independence scenario and  for the statistical-dependence scenario, only the umbrella correlation estimators under self-normalized importance sampling for the pair of random variables  are provided in Figure 36. The approximate theoretical distribution (see Section 7.5 for details) under regular sampling is more peaked for  than for , which follows by comparing Figure 36A and Figure 36B. For example, the approximate width of the theoretical estimator density in Figure 36A is  and in Figure 36B equals . Of course, the width of these estimator distributions (both empirical or theoretical) reduces when the sample size  is increased from the value  in Figure 36. That being said, the spread in the correlation estimations that can occur in a small sample of size  is perhaps surprising. Comparing Figure 36B to Figure 36A, it does appear that the performance of the correlation umbrella estimator under self-normalized importance sampling for the analysis scenario  in Figure 36B is outperformed by the performance in Figure 36A, albeit both figure panels demonstrate a reasonable performance for all intents and purposes.

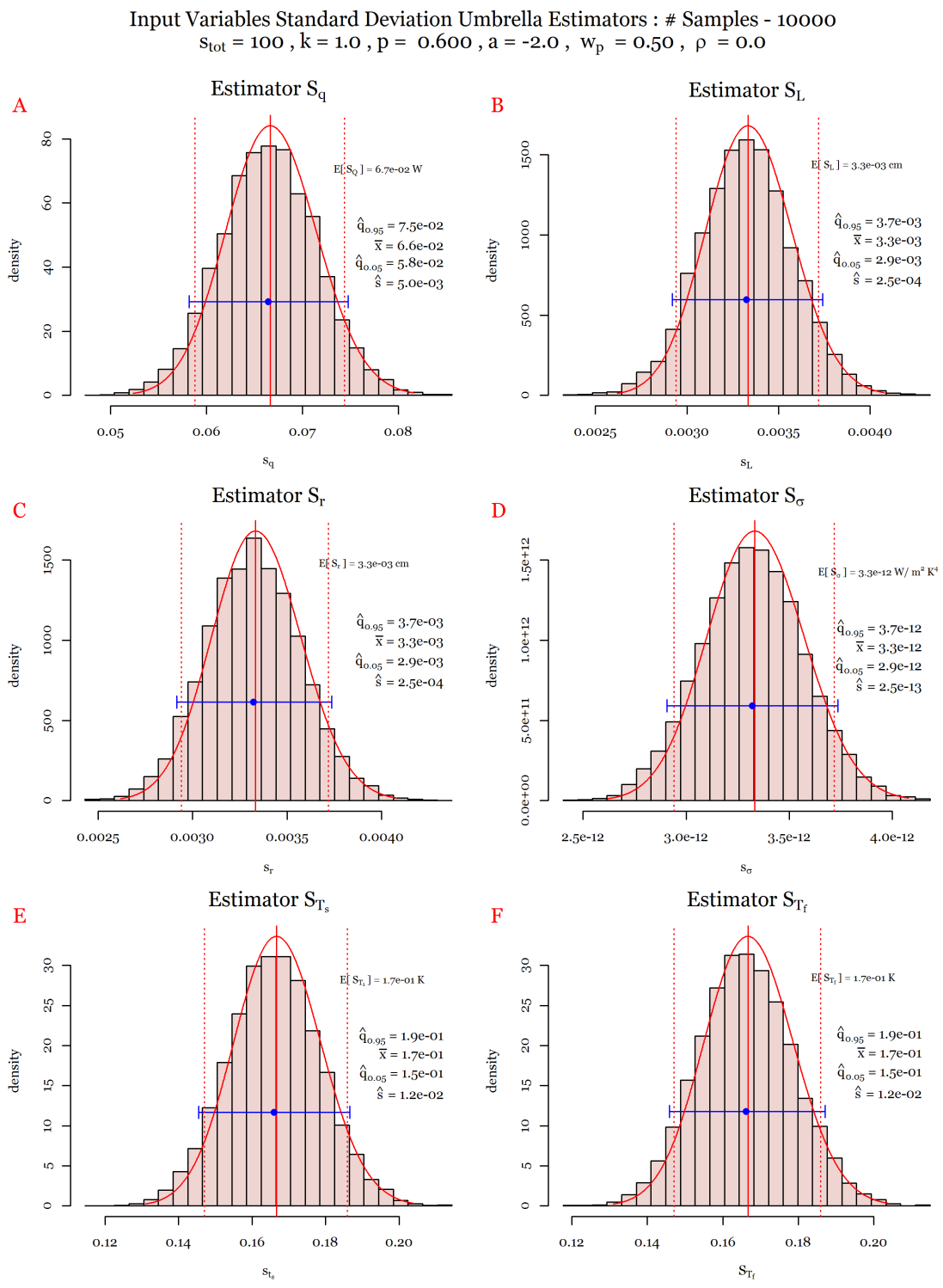


Figure 34. Comparison of theoretical and empirical standard-deviation estimator distributions for the input variables in Table 1 under regular sampling and umbrella sampling, using self-normalized importance weights for the analysis scenario .

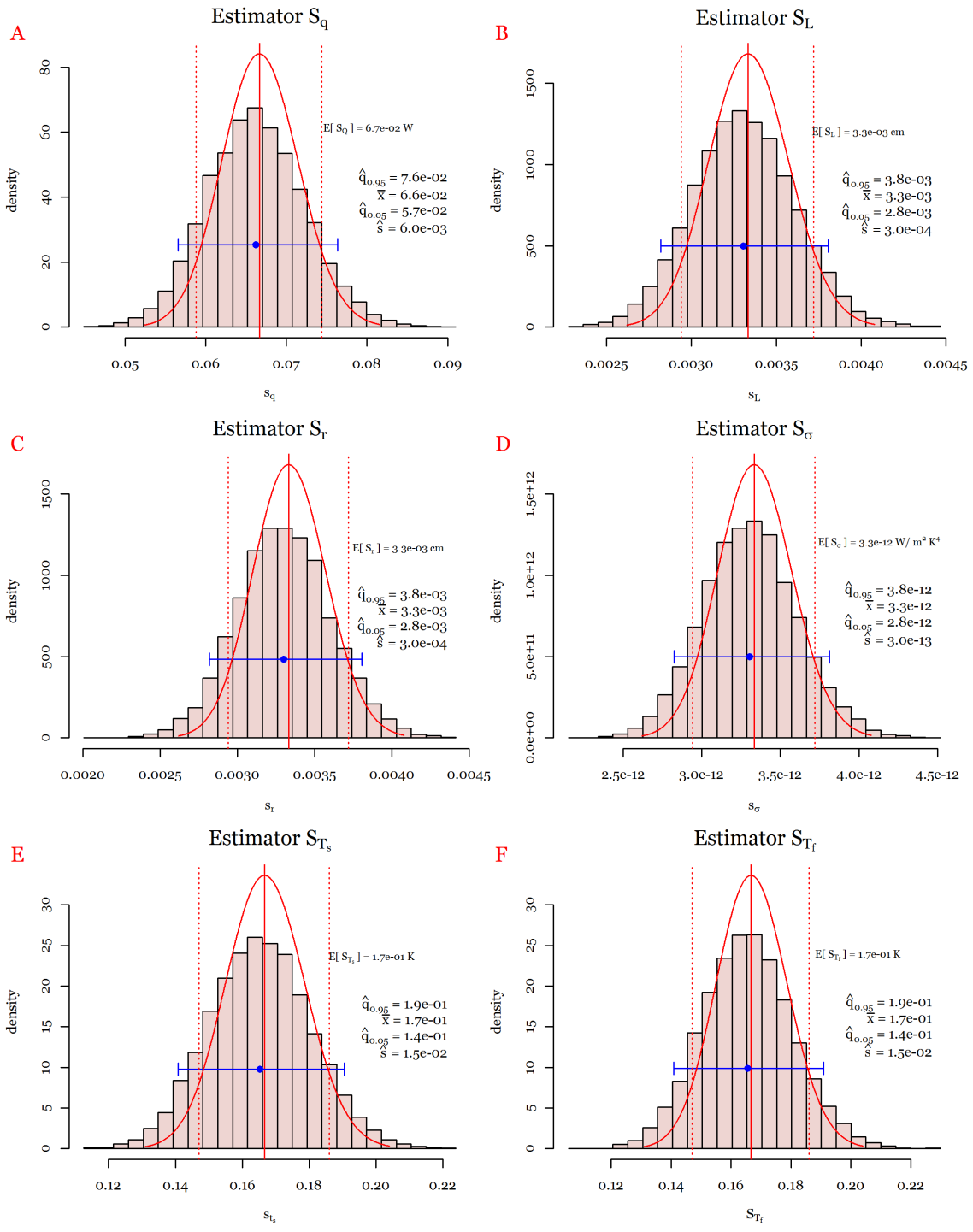


Figure 35. Comparison of theoretical and empirical standard-deviation estimator distributions for the input variables in Table 1 under regular sampling and umbrella sampling using self-normalized importance weights for the analysis scenario .

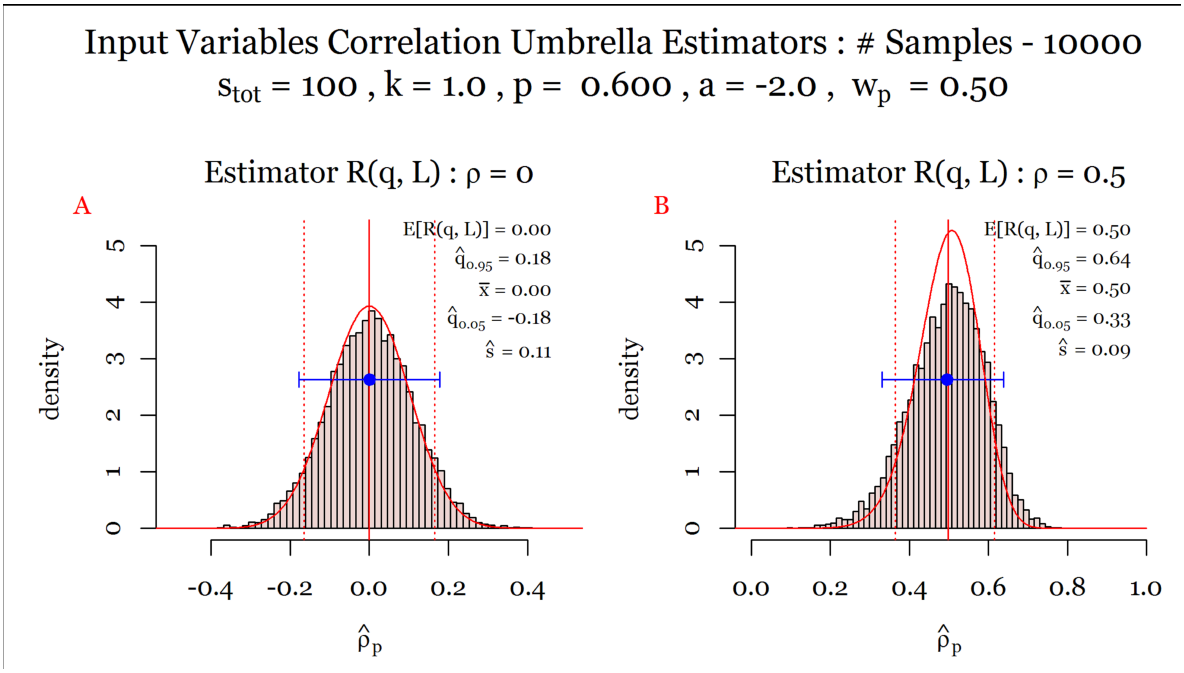


Figure 36. Comparison of and approximated theoretical and empirical-correlation estimator distributions for the input variables and in Table 1 under regular sampling and umbrella sampling using self-normalized importance weights. A: Analysis scenario ; B: Analysis scenario .

### 8.2.2 Emissivity Umbrella Estimates

Having established reasonable umbrella-estimator behavior for the input variables in Table 1 under self-normalized importance sampling given umbrella sampling parameters and , the next step is to evaluate emissivity samples from and an input sample of size . Figure 37 plots the empirical cdf (in dark red) of a single instance of sample of emissivity of size , evaluated using and an umbrella input sample of size with —i.e., under statistical independence of the input random variables as per the umbrella-sampling procedure developed. For comparison purposes, Figure 37 also plots empirical cdf (in blue color) evaluated under regular sampling using a regular sample of size . Finally, Figure 37 also plots the Wilks empirical cdf (in orange), evaluated under regular sampling (also plotted in Figure 31) using a regular sample of size . Comparing the three empirical cdfs in Figure 37, one concludes that the empirical cdf in dark red, using only , is heavier tailed than the empirical cdfs plotted in orange and blue, using samples and , respectively. This was, of course, the purpose of developing the umbrella-sampling approach. Specifically, the objective was the construction of a sampling procedure that ensures a larger number of samples in the tails of an output distribution while demonstrating reasonable performance of mean and standard-deviation estimation behavior using importance weights.

Figure 37 provides the mean umbrella estimate for emissivity in dark red and in blue, obtained using samples. The mean emissivity was estimated at in Table 2 from a sample of size .

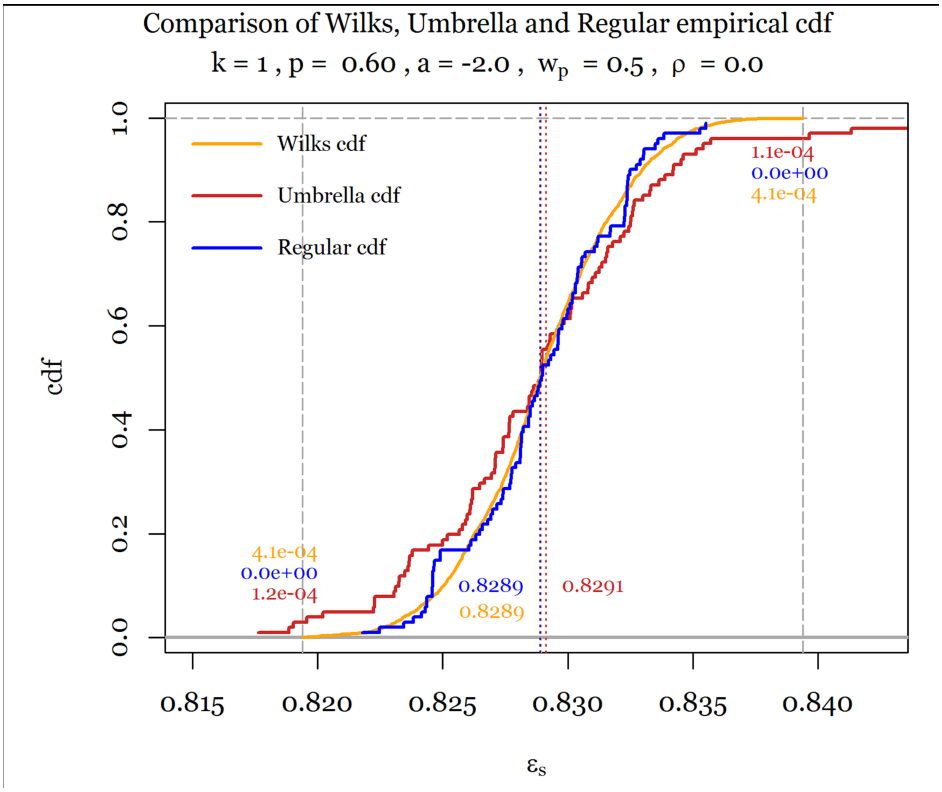


Figure 37. Comparison of Wilks empirical emission cdf (in orange) from Figure 31, an umbrella empirical emission cdf (in dark red) and an empirical emission cdf (in blue) both obtained from multivariate input samples and for the analysis scenario .

Their three values are also plotted using vertical dashed lines in the same color as the empirical cdfs. These show close alignment among all three estimates. Moreover, Figure 37 provides the umbrella lower-tail probability estimate , where is the smallest order statistic obtained using the Wilks method sample of size (plotted using a vertical dashed gray line in Figure 37). One evaluates from that regular sample of size a left-tail probability estimate , plotted in orange in Figure 37. The difference in these estimates is of course that the first one () is evaluated utilizing only umbrella samples while the second one () is evaluated using regular samples, which is a reduction in sample size of . In fact, under regular sampling using a sample size of , a left-tail probability estimate results in Figure 37, which is plotted in blue.

Finally, Figure 37 also provides the umbrella upper-tail probability estimate , where is the largest-order statistic obtained using the Wilks method sample of size (also plotted using a vertical dashed line in a gray color in Figure 37). The upper-tail probability estimate using the same sample size , but under regular sampling, also results in the value zero (plotted in blue). The upper-tail probability estimate under regular sampling using samples is the same as that of the lower-tail probability and is estimated at , plotted an orange.

Figure 38 is analogous to Figure 37 and plots the empirical cdf in dark red of a single instance of sample of emissivity evaluated using , obtained using a multivariate umbrella input sample of size with —i.e. under a positive dependence scenario of the six input random variables in Table 1. Figure 38 also plots the empirical cdf (in green) evaluated under regular sampling (also plotted in Figure 31, in the same color) using a regular sample of size , and one in blue, under regular sampling, using a sample size . One observes from Figure 38 perhaps a slightly heavier-tailed empirical umbrella cdf than in Figure 37. That being said, both the lower-tail probability umbrella estimate, , and the upper-tail probability umbrella estimate, , are higher and lower, respectively, than the estimates in Figure 37. Of course, this is, in part, a

result of different importance weights in the umbrella sampling procedure for the analysis scenarios  and , respectively. As in Figure 37, one observes a close alignment between the umbrella mean-emissivity estimate  (in dark red), the mean-emissivity estimate  provided in Table 2 for the analysis scenario  (in dark green), and the mean emissivity estimate  (in blue) obtained using a regular sample of size . Note that, under regular sampling, as in Figure 37, a sample size of  results in tail-probability estimates valued at zero (plotted in blue in Figure 38).

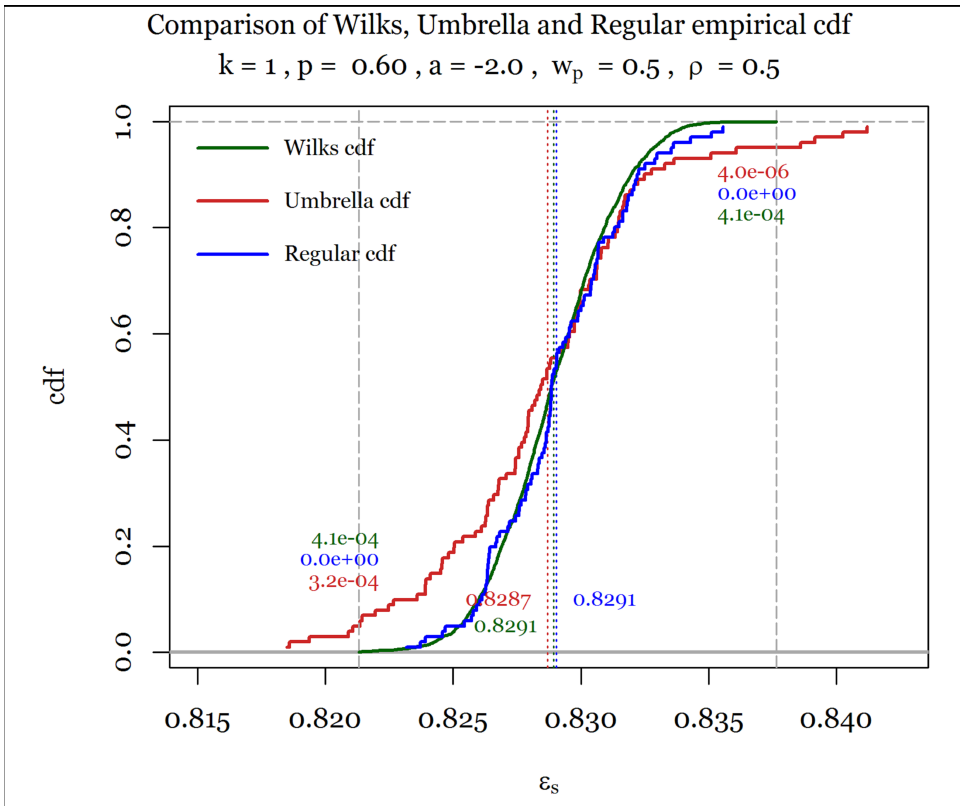


Figure 38. Comparison of Wilks empirical emission cdf (in green) from Figure 31, an umbrella empirical emmision cdf (in dark red), and an empirical emission cdf (in blue) obtained from  multivariate input samples and  for the analysis scenario .

### 8.2.3 Emissivity Umbrella-Estimator Behavior

Figure 37 and Figure 38 are examples of single instances for an umbrella sample of emissivity  of size . Of course, the mean, standard deviation, and tail-probability umbrella estimates vary from instance to instance, in particular with such a small sample size. Recall that to obtain a single-instance estimate, one first generates a multivariate input sample of size ; second, one evaluates an emissivity output sample of the same size, as per , for each input sample, and third, one evaluates a realization of either the umbrella estimator or regular estimator using the  emissivity values obtained, either via umbrella sampling or regular sampling. The variability in these estimates is obtained by plotting their estimator distributions empirically. Because the theoretical estimator distribution for emissivity under regular sampling is unknown, the empirical estimator distributions under both umbrella and regular sampling, using the same sample size , are compared.

Figure 39A plots the empirical-estimator distribution for mean emissivity , obtained using  mean estimates obtained from  emissivity output samples in the manner described above for the analysis scenario  under regular MVN sampling.

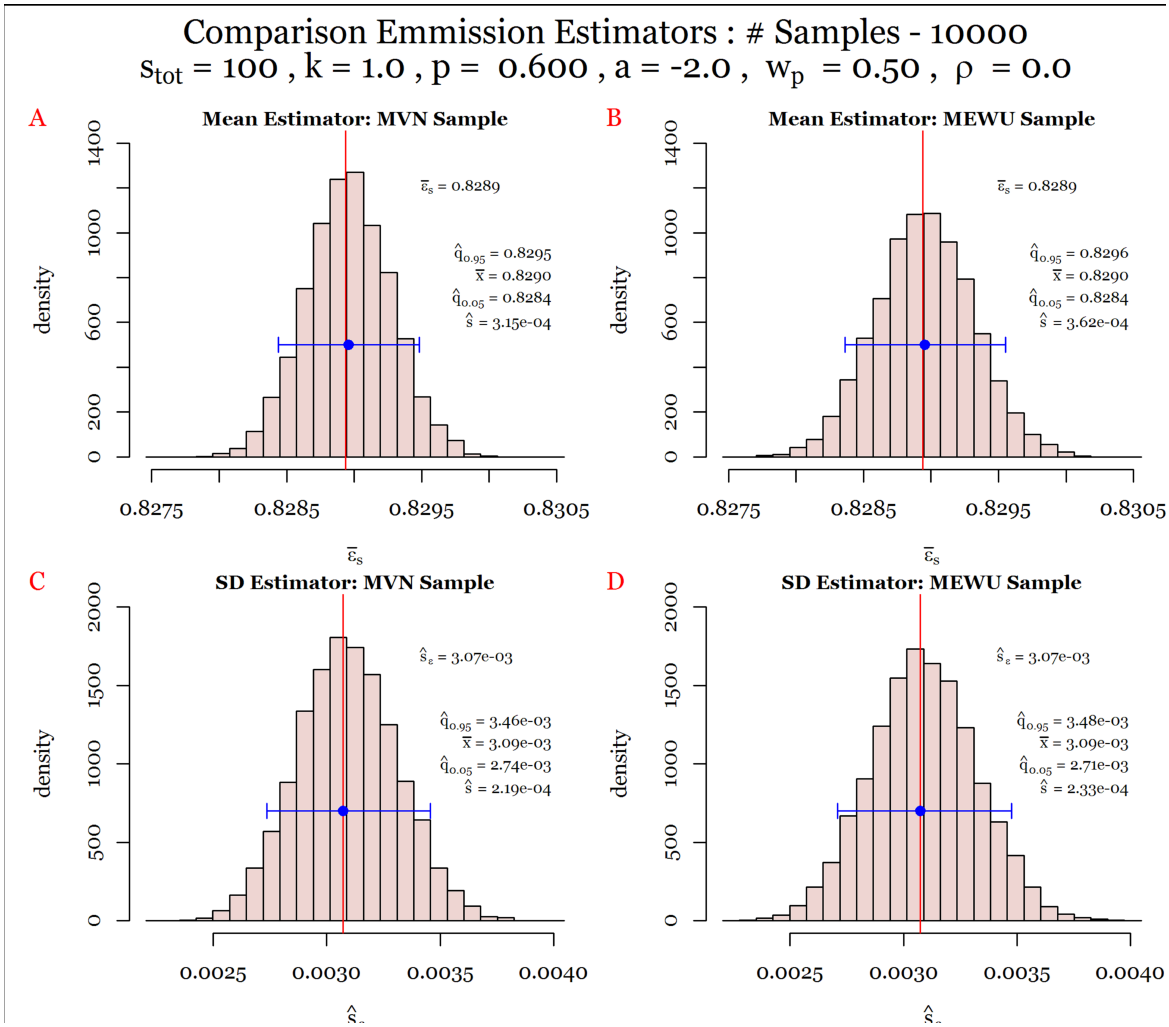


Figure 39. Empirical mean and standard-deviation regular- and umbrella-estimator distributions for emissivity for the analysis scenario . A: MVN mean estimator; B: Multivariate equal weighted umbrella (MEWU) mean estimator; C: MVN standard deviation estimator; D: MEWU standard deviation estimator.

Figure 39B plots the empirical estimator distribution for mean emissivity under MEWU sampling. The vertical red lines in Figure 39A and Figure 39B are plotted at the mean estimates provided in Table 2 obtained using a regular MVNinput sample of size . One observes a close alignment between the empirical mean values of the estimators and the vertically plotted solid red lines in Figure 39A and Figure 39B. In further comparing Figure 39A and Figure 39B, one observes a slightly larger standard deviation of the mean estimator under MEWU sampling. The blue error bars of the mean estimator distributions in Figure 39A and Figure 39B, however, are close in value.

Figure 39C plots the empirical-estimator distribution for the standard deviation of emissivity for the same analysis scenario, , under MVN sampling using a sample size of . Figure 39D plots the empirical-estimator distribution for the standard deviation of emissivity for the same analysis scenario, , under MEWU sampling using that same sample size of . The vertical red lines in Figure 39C and Figure 39D are plotted at the standard-deviation estimates provided in Table 2 for the analysis scenario obtained using regular MVN input samples. Here too, one observes a close alignment between the empirical mean values of the estimators and the vertically plotted solid red lines in Figure 39C and Figure 39D. The blue error bars in Figure 39C and Figure 39D, as before, plot the empirical mean values of the estimators at the blue

solid dot and the empirically estimated  and  percentiles. These empirically estimated quantiles in Figure 39C and Figure 39D are close in value, but slightly wider in Figure 39D. This, too, is evidenced by a slightly larger standard deviation of the estimator distribution under MEWU sampling in Figure 39D than the estimator distribution plotted in Figure 39C under regular MVN sampling.

Figure 40 is analogous to Figure 39, but was evaluated for the analysis scenario . In comparing the mean estimator distributions in Figure 40A and Figure 40B, one observes perhaps a lesser performance in Figure 40B than in Figure 39B for the analysis scenario . That being said, the mean values in the blue error bars align well with the solid vertical red lines, which are plotted at the mean-value estimates for the analysis scenario  in Table 2. Moreover, a comparison of the empirical  and  percentiles in Figure 40A (evaluated from MVN samples) to the ones in Figure 40B (evaluated from MEWU samples), show that they are close in value. Similar conclusions can be drawn when comparing Figure 40C and Figure 40D, which plot the empirical standard-deviation estimator distributions under MVN sampling and MEWU sampling, respectively. Again, one observes a close alignment with the mean values of the blue error bars and the standard-deviation estimates provided in Table 2 and obtained from  MVN samples.

Summarizing, the comparison of umbrella-estimator distributions for the mean and standard deviations in Figure 39 and Figure 40 to the traditional-estimator distributions obtained under regular sampling, a reasonable performance is observed for the umbrella-estimator distributions.

Finally, Figure 41 plots the empirical-estimator distribution of the combined-tail probability estimators under MVN sampling and MEWU sampling using self-normalized importance weights for both the analysis scenarios  (Figure 41A and Figure 41B) and  (Figure 41C and Figure 41D). Each of the tail-probability estimates used to generate Figure 41A and Figure 41C are obtained using  MVN samples.

In fact, the estimator distributions in Figure 41B and Figure 41D display a continuous—i.e., non-degenerate—estimator behavior using only  samples to estimate the tail probabilities beyond the extremes provided in Table 2. The latter is further evidence of the empirical emissivity umbrella cdf instances, of which one is displayed in red in Figure 37 and one in Figure 38, being heavier tailed than the Wilks cdfs displayed in Figure 31, despite using only  samples. It is that heavier-tailed behavior, combined with self-normalized importance weights from the MEWU sampling approach, that results in the improved emissivity tail-probability estimator behavior in Figure 41C and Figure 41D, compared to the degenerate estimator distribution in Figure 41A and Figure 41C.

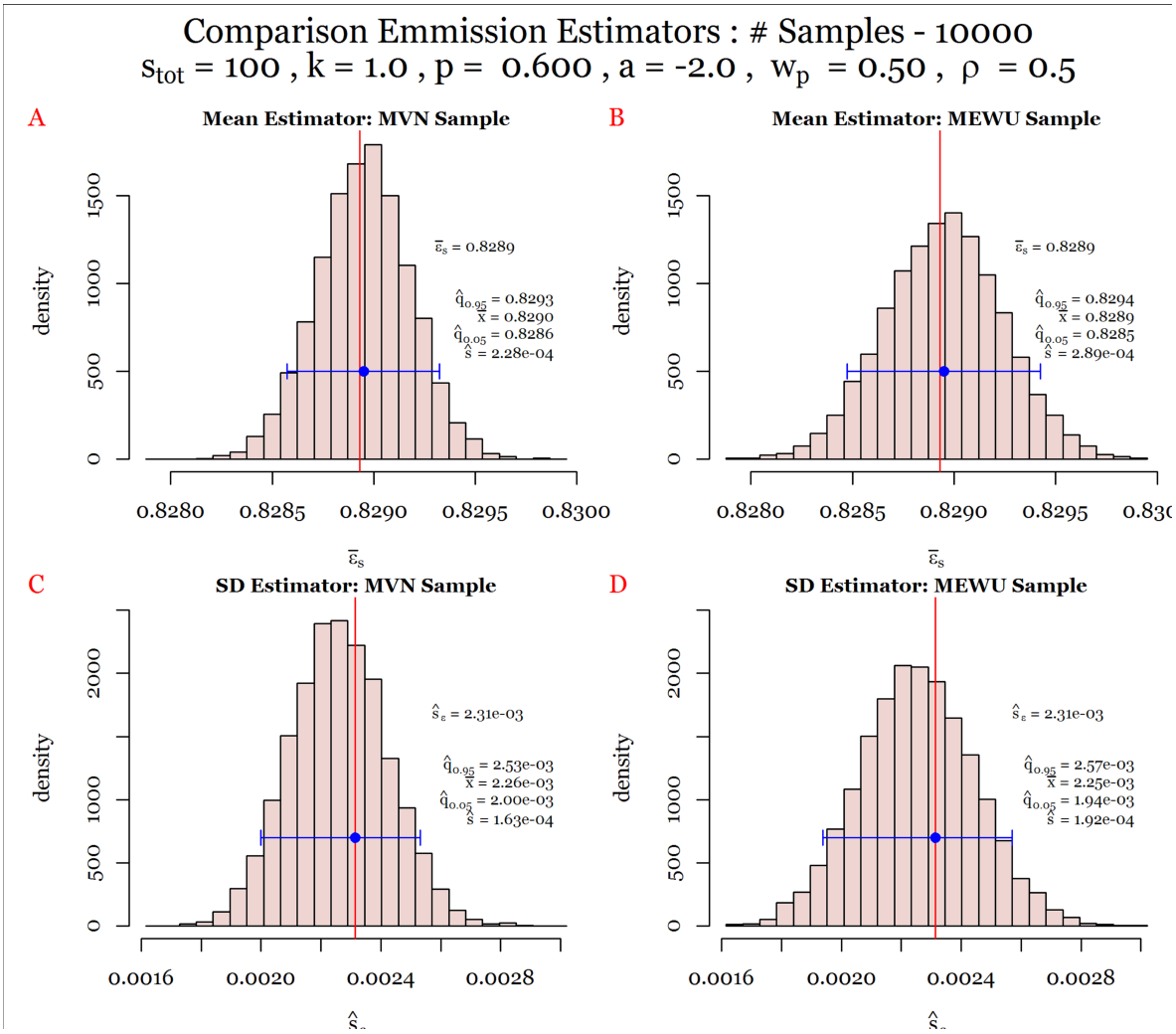


Figure 40. Empirical mean and standard-deviation regular- and umbrella-estimator distributions for emissivity for the analysis scenario . A: MVN mean estimator; B: MEWU mean estimator; C: MVN standard deviation estimator; D: MEWU standard deviation estimator.

Observe that the resulting estimator distributions in Figure 41A and Figure 41C are degenerate distributions, with most of their probability mass located at the value zero and some at the value , indicating a single sample's (out of ) falling outside the extremes plotted as dashed vertical gray lines in Figure 37 and Figure 38. Note that in Figure 41C the and empirical quantiles are both equal to the value zero. On the other hand, in Figure 41A, the percentile is equal to the value .

A stark difference is observed when the estimator distribution under MEWU sampling is compared, in Figure 41B and Figure 41D, to the estimator distributions in Figure 41A and Figure 41B. The extreme tails probability in Table 2—i.e., —is plotted using solid vertical red lines in Figure 41. One observe from the blue dot of the error bar an over-estimation of that extreme-tails probability in Figure 41B and an underestimation in Figure 41C. The latter can be explained by the realization that a six-dimensional input sample of relatively small size was used, combined with , to obtain an emissivity sample of size , from which, in turn, a small extreme-tails probability was estimated. There is no doubt that estimation behavior would improve when increasing the sample size. Finally, a larger standard deviation is observed for the analysis scenario in Figure 41B than for the analysis scenario in Figure 41D.

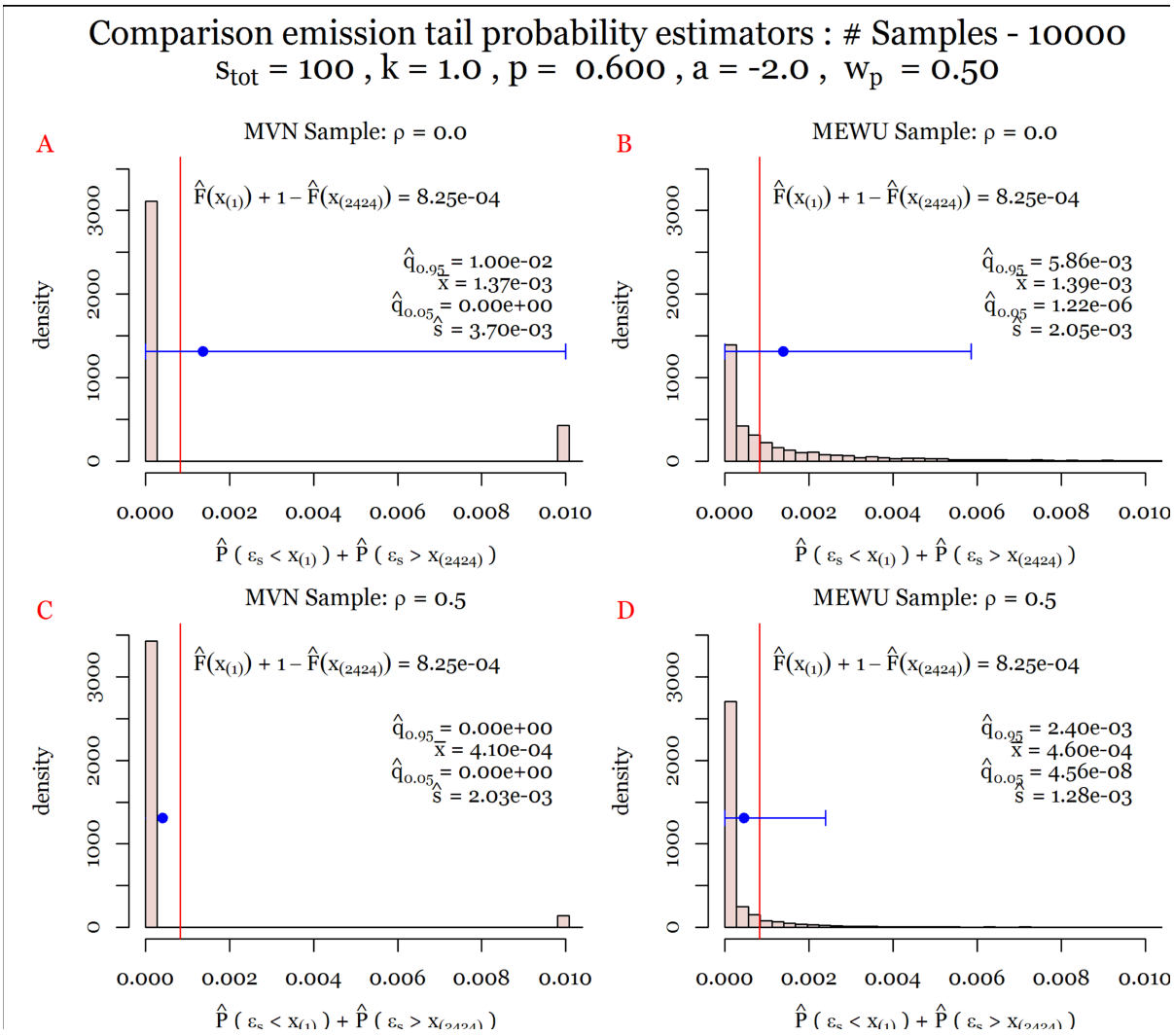


Figure 41. Empirical tail-probability estimators for emissivity under regular MVN sampling and MEWU sampling using self-normalized importance weights. A: MVN sampling scenario ; B: MEWU sampling scenario ; C: MVN sampling scenario ; D: MEWU sampling scenario .

# 9. CONCLUSION

Summarizing, the equally weighted multivariate umbrella-sampling procedure developed in Section 7.4, designed for multivariate normal distributions using multivariate gamma tails as constructed in Section 7.1, combined with importance estimation as presented in Section 4, allows for robustness of various estimator behaviors under a small sample size of  while ensuring that, in that small sample size, the tails of the distribution of interest are visited more often than under regular sampling. The latter was the objective of this research project. The robust performance of mean and variance estimators was demonstrated for the equally weighted marginal umbrella pdfs with gamma tails in Section 6.4. The umbrella estimation procedures were demonstrated in an engineering uncertainty analysis example in Section 8.

It is worth mentioning that the generation of stochastic data as part of the stochastic/robust optimzation process currently implemented in RAVEN uses the ARMA (Auto Regressive Moving Average) methodology. The sampling methodology developed herein might be of value in the evaluation of those low probabilty, high consequence scenarios in the calculation of the system's net present value.

# 10. REFERENCES


[1] Shannon Bragg-Sitton, Richard D. Boardman, Cristian Rabiti, James O'Brien. 2020. “Reimagining future energy systems: Overview of the U.S. program to maximize energy utilization via integrated nuclear-renewable energy systems. International Journal of Energy Research 44(10).

[2] Brown Maxwell, Wesley Cole, Kelly Eurek, Jon Becker, David Bielen, Ilya Chernyakhovskiy, Stuart Cohen, et al. 2020. Regional Energy Deployment System (ReEDS) Model Documentation: Version 2019. Golden, CO: National Renewable Energy Laboratory. NREL/TP-6A20-74111.

[3] Watson, Jean Paul, Knueven, Bernard, Concepcion, Ricky, Melander, Darryl, Short, Austin, Zhang, Pengchu, and Woodruff, David. PRESCIENT. Computer Software. https://github.com/grid-parity-exchange/Prescient. USDOE. 11 May. 2020. Web. doi:10.11578/dc.20201101.1.

[4] Paul W. Talbot Cristian Rabiti Andrea Alfonsi Cameron Krome M. Ross Kunz Aaron Epiney Congjian Wang Diego Mandelli. 2020. Correlated synthetic time series generation for energy system simulations using Fourier and ARMA signal processing, https://doi.org/10.1002/er.5115

[5] Chao Yan, Tao Ding, Zhaohong Bie, and Xifan Wang. A geometric programming to importance sampling for power system reliability evaluation. IEEE Transactions on Power Systems, 32(2):1568–1569, 2016.

[6] Dougal HO McQueen, Patrick R Hyland, and Simon J Watson. Monte carlo simulation of residential electricity demand for forecasting maximum demand on distribution networks. IEEE Transactions on power systems, 19(3):1685–1689, 2004.

[7] Edinaldo José da Silva Pereira, João Tavares Pinho, Marcos André Barros Galhardo, and Wilson Negrão Macêdo. Methodology of risk analysis by monte carlo method applied to power generation with renewable energy. *Renewable Energy*, 69:347–355, 2014.

[8] Alexander J McNeil. Estimating the tails of loss severity distributions using extreme value theory. ASTIN Bulletin: The Journal of the IAA, 27(1):117–137, 1997.

[9] Florentina Paraschiv, Risto Hadzi-Mishev, and Dogan Keles. Extreme value theory for heavy tails in electricity prices. Journal of Energy Markets, 9(2), 2016.

[10] Christina Steinkohl, Richard A Davis, and Claudia Klüppelberg. Extreme value analysis of multivariate high-frequency wind speed data. Journal of Statistical Theory and Practice, 7(1):73–94, 2013.

[11] Perwez Shahabuddin Paul Glasserman, Philip Heidelberger. Variance reduction techniques for estimating value-at-risk. Management Science, 46(3):1485–1493, 2000.

[12] Herman Kahn and Theodore E Harris. Estimation of particle transmission by random sampling. National Bureau of Standards applied mathematics series, 12:27–30, 1951.

[13] J.P.C. Hopmans, A.C.M.; Kleijnen. Importance sampling in systems simulation: A practical failure? Mathematics and Computers in Simulation, 21(2):209–220, 1979.

[14] Tim Hesterberg. Weighted average importance sampling and defensive mixture distributions. *Technometrics*, 37(2):185–194, 1995.

[16] Art Owen and Yi Zhou. Safe and effective importance sampling. Journal of the American Statistical Association, 95(449):135–143, 2000.

[17] Herman Kahn and Andy W Marshall. Methods of reducing sample size in monte carlo computations. Journal of the Operations Research Society of America, 1(5):263–278, 1953.

[18] R Core Team. R: A Language and Environment for Statistical Computing. R Foundation for Statistical Computing, 2017.

[19] Guido Rossum. Python reference manual. CWI (Centre for Mathematics and Computer Science), 1995.

[20] Luca Martino, Victor Elvira, and Francisco Louzada. Effective sample size for importance sampling based on discrepancy measures. Signal Processing, 131:386–401, 2017.

[21] Harry Joe. Multivariate models and multivariate dependence concepts. CRC Press, 1997.

[22] Ronald A Fisher. Frequency distribution of the values of the correlation coefficient in samples from an indefinitely large population. *Biometrika*, 10(4):507–521, 1915.

[25] Richard A Davis. Practical numerical methods for chemical engineers: Using Excel with VBA. CreateSpace Independent Publishing Platform, 2018.

[26] David Halliday, Robert Resnick, Jearl Walker, et al. Electric fields. Fundamentals of physics, pages 580–604, 2005.

[27] C. Kittel and H. Kroemer. Thermal physics. American Association of Physics Teachers, 1998.

[28] William R Corliss. Nuclear Reactors for Space Power, Understanding the Atom Series. ERIC, 1971.

[29] Johan R Van Dorp, Ekundayo Shittu, and Christian Rabiti. A two-quantile constraint wilks' method with applications in energy engineering uncertainty analysis. Unpublished Manuscript, 2021.

[30] Geoff Tennant. Six Sigma: SPC and TQM in Manufacturing and Services. Taylor & Francis, 2017.

[23] Fisher, R.A., 1915. Frequency distribution of the values of the correlation coefficient in samples from an indefinitely large population. Biometrika, 10(4), pp.507-521.

[24] Fisher, R.A., 1921. On the'probable error'of a coefficient of correlation deduced from a small sample. Metron, 1, pp.1-32.

[15] Huang, J., Xue, Y., Dong, Z.Y. and Wong, K.P., 2012. An efficient probabilistic assessment method for electricity market risk management. IEEE Transactions on Power Systems, 27(3), pp.1485-1493.

[31] Art B. Owen. Monte Carlo theory, methods and examples. 2013.